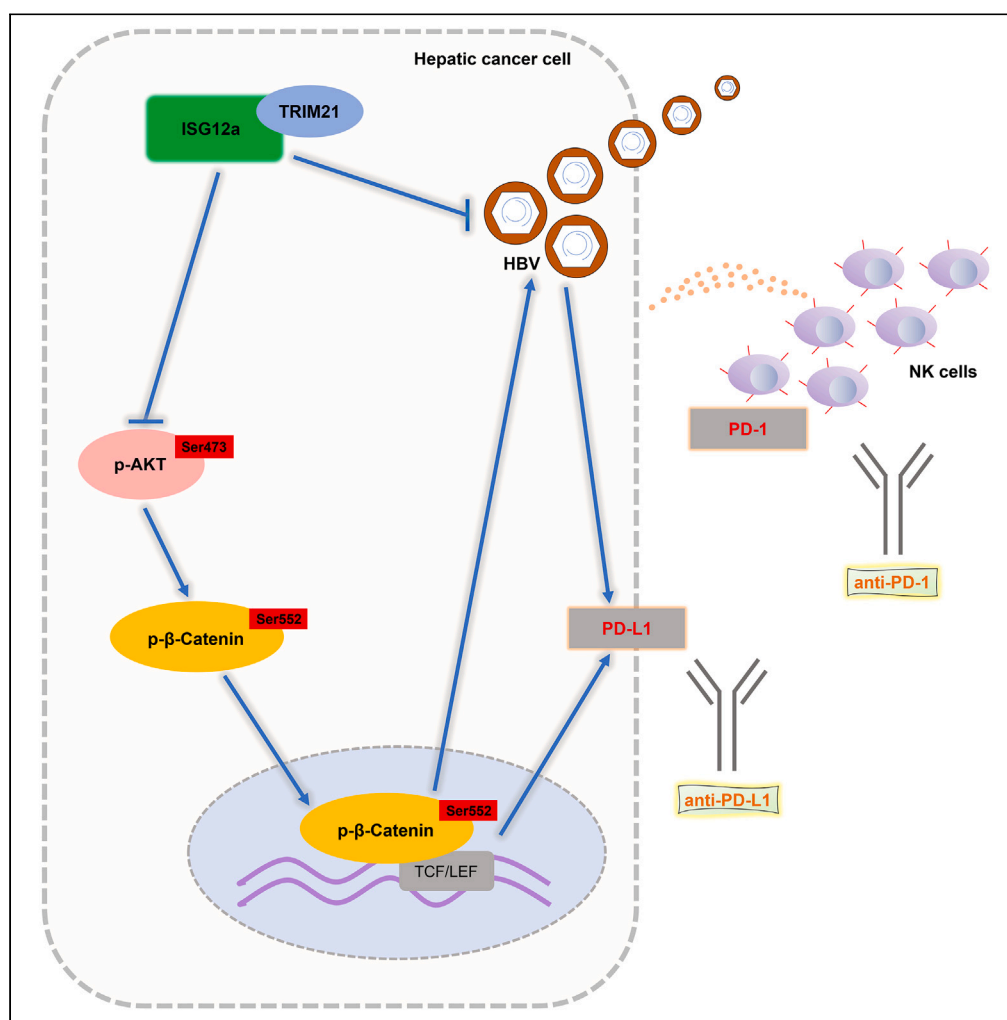


## Article

ISG12a promotes immunotherapy of HBV-associated hepatocellular carcinoma through blocking TRIM21/AKT/ $\beta$ -catenin/PD-L1 axis

Rilin Deng, Renyun Tian, Xinran Li, ..., Binbin Xue, Chaohui Zuo, Haizhen Zhu

hy0206218@hainmc.edu.cn

## Highlights

Low expression of ISG12a predicts poor prognosis of HBV-associated HCC

High expression of tumor intrinsic ISG12a indicates active NK cell phenotypes

ISG12a inhibits PD-L1 expression by regulating TRIM21-AKT- $\beta$ -catenin signal axis

Tumor intrinsic ISG12a promotes NK cell immunosurveillance against HBV-associated HCC

## Article

ISG12a promotes immunotherapy of HBV-associated hepatocellular carcinoma through blocking TRIM21/AKT/ $\beta$ -catenin/PD-L1 axis

Rilin Deng,<sup>1,2,3,6</sup> Renyun Tian,<sup>1,2,6</sup> Xinran Li,<sup>1</sup> Yan Xu,<sup>1</sup> Yongqi Li,<sup>4</sup> Xintao Wang,<sup>1</sup> Huiyi Li,<sup>1,2</sup> Luoling Wang,<sup>1</sup> Biaoming Xu,<sup>5</sup> Di Yang,<sup>1</sup> Songqing Tang,<sup>1</sup> Binbin Xue,<sup>1,2</sup> Chaohui Zuo,<sup>5</sup> and Haizhen Zhu<sup>1,2,7,\*</sup>

## SUMMARY

**Hepatitis B virus (HBV) infection generally elicits weak type-I interferon (IFN) immune response in hepatocytes, covering the regulatory effect of IFN-stimulated genes. In this study, low level of IFN-stimulated gene 12a (ISG12a) predicted malignant transformation and poor prognosis of HBV-associated hepatocellular carcinoma (HCC), whereas high level of ISG12a indicated active NK cell phenotypes. ISG12a interacts with TRIM21 to inhibit the phosphorylation activation of protein kinase B (PKB, also known as AKT) and  $\beta$ -catenin, suppressing PD-L1 expression to block PD-1/PD-L1 signaling, thereby enhancing the anticancer effect of NK cells. The suppression of PD-1-deficient NK-92 cells on HBV-associated tumors was independent of ISG12a expression, whereas the anticancer effect of PD-1-expressed NK-92 cells on HBV-associated tumors was enhanced by ISG12a and treatments of atezolizumab and nivolumab. Thus, tumor intrinsic ISG12a promotes the anticancer effect of NK cells by regulating PD-1/PD-L1 signaling, presenting the significant role of innate immunity in defending against HBV-associated HCC.**

## INTRODUCTION

People who infected with hepatitis B virus (HBV) may suffer from cirrhosis, liver failure, and liver cancer, and 90% of primary liver cancers are hepatocellular carcinoma (HCC).<sup>1</sup> Due to the stealthy of HBV infection and the difficulty in early detection, most HCC are diagnosed at the late stages. However, effective methods for therapy of the advanced HCC are limited at present. For these reasons, the 5-year overall survival rate of HCC is only 18%, which is even lowered to less than 12.5% in China.<sup>2</sup> Studying the behind mechanism are of great value for improving the efficacy of early diagnosis and curative therapies for HBV-associated HCC.

Vaccination is essential to prevent HBV infection, but human beings who have been infected with HBV and those who have not been vaccinated are at high risks for suffering from HBV-associated HCC. Sorafenib and lenvatinib are the merely first-line drugs approved for therapy of the advanced HCC with limited survival benefit but obvious side effects.<sup>3</sup> HBV infection induces immune imbalance for HCC progression,<sup>4,5</sup> and the high level of PD-1 and PD-L1 may predict the development and progression of HCC.<sup>6,7</sup> PD-1/PD-L1 signaling is an underlying mechanism for explaining the immune evasion of HBV-associated HCC. Nivolumab and pembrolizumab have been approved as the second-line therapies for unresectable HCC following the therapeutic failure of sorafenib.<sup>8,9</sup> Other immune checkpoint blockades (ICBs) represented by ipilimumab and combination therapies such as durvalumab with tremelimumab, and pembrolizumab with lenvatinib have been approved for advanced and unresectable HCC.<sup>10</sup> However, the complexity of cancer heterogeneity and tumor microenvironment limits the therapeutic efficacy of ICBs.

Natural killer (NK) cells are immune cells with innate cytolytic ability, participating in immune surveillance against cancer, and viral infection. The downregulated major histocompatibility complex class I (MHC class I) molecules limits the anticancer effect of T cells. However, NK cells may recognize cancer cells according to the downregulated MHC class I molecules, thereby secreting perforin and granzymes or expressing tumor necrosis factor (TNF)-related apoptosis inducing ligand (TRAIL) and FasL to exert cytotoxic effects or producing interferons (IFNs) to

<sup>1</sup>Institute of Pathogen Biology and Immunology, College of Biology, State Key Laboratory of Chemo/Biosensing and Chemometrics, Hunan University, Changsha 410082, Hunan, China

<sup>2</sup>Key Laboratory of Tropical Translational Medicine of Ministry of Education, Department of Pathogen Biology, School of Basic Medicine and Life Science, Department of Clinical Laboratory of the Second Affiliated Hospital, The University of Hong Kong Joint Laboratory of Tropical Infectious Diseases, The Second Affiliated Hospital of Hainan Medical University, Hainan Medical University, Haikou 571199, Hainan, China

<sup>3</sup>Hunan Normal University School of Medicine, Changsha 410013, Hunan, China

<sup>4</sup>Institute of Translational Medicine, The First Hospital of Jilin University, Changchun 130031, Jilin, China

<sup>5</sup>Department of Gastrointestinal and Pancreatic Surgery, Translational Medicine Joint Research Center of Liver Cancer, Laboratory of Digestive Oncology, Hunan Cancer Hospital & The Affiliated Cancer Hospital of Xiangya School of Medicine, Central South University, Clinical Research Center For Tumor of Pancreaticobiliary Duodenal Junction In Hunan Province, Changsha 410013, Hunan, China

<sup>6</sup>These authors contributed equally

<sup>7</sup>Lead contact

\*Correspondence: [hy0206218@hainmc.edu.cn](mailto:hy0206218@hainmc.edu.cn)

<https://doi.org/10.1016/j.isci.2024.109533>



activate macrophages and T cells.<sup>11</sup> With the publication of the first clinical trial of chimeric antigen receptor (CAR)-engineered natural killer (CAR-NK) cells targeting CD19-positive lymphoma (NCT03056339),<sup>12</sup> NK cell therapy has become a new focus in cancer immunotherapy for the high efficacy and safety. Primary NK cells, NK cell lines represented by NK-92, adaptive NK cells, cytokine induced memory like NK cells, and CAR-NK cells are main sources of therapeutic NK cells in clinical trials.<sup>13</sup> IL-2 dependent NK-92 cells are defective in PD-1 and CD16 expression, but have active NK cell function and phenotypes and have been clinically used in advanced cancer.<sup>14,15</sup>

The expression level of inflammatory factors, represented by IFNs, is downregulated in progression of chronic HBV infection, leading to HBV replication and immune evasion of HBV-associated HCC.<sup>16,17</sup> IFNs perform sustained suppression on HBV replication, contributing to restoration of innate responses and/or via production of antiviral IFN stimulated genes (ISGs).<sup>18</sup> In our study of innate immunity, IFN-stimulated gene 12a (ISG12a) has been identified with great potential on inhibiting viral infection and malignances: promoting the innate immune response of host cells to newcastle disease virus (NDV) infection,<sup>19</sup> restricting the infection of hepatitis C virus (HCV),<sup>20</sup> enhancing anticancer immunity by inhibiting the Wnt/ $\beta$ -catenin signaling pathway,<sup>21</sup> and inducing pyroptosis in virus-infected cancer cells.<sup>22</sup> The antiviral and anticancer effects make ISG12a an innate immune effector. However, direct evidence for relationship between immune regulation of ISG12a and immune surveillance of NK cells in cancer is still lacking. This study mainly explored the regulatory effect and mechanism of tumor intrinsic ISG12a on immune surveillance of NK cells in HBV-associated HCC, which may provide sights for improving the immunotherapeutic efficacy.

## RESULTS

### ISG12a inhibits PD-L1 expression and cancer phenotypes in HBV-infected hepatic cancer cells

HBV infection generally elicits weak type-I IFN immune response in hepatocytes, covering the regulatory effect of IFN signaling and ISGs on HBV-associated HCC.<sup>23</sup> Here, we uncovered that the levels of p-STAT1 and p-STAT2 in HLCZ01 cells was almost unchanged with HBV infection while increased by NDV infection (Figure 1A), approving the previous point. Hepatic cancer cells HLCZ01 support the entire life cycle of HBV-produced both in cell culture and clinically,<sup>24</sup> functioning as a promising tool for exploring HBV-associated HCC. Through conducting *in vitro* and *in vivo* experiments, we firstly determined the feasibility of HLCZ01 cells for studying HBV-associated HCC. Interestingly, the levels of p-AKT (Ser473) and p-mTOR (Ser2448) in HLCZ01 cells were upregulated with the infection of HBV (HLCZ01 + HBV) (Figure 1B). Notably, the level of glycosylated PD-L1 (hereinafter called PD-L1) on surface of HLCZ01 cells was also increased (Figures 1B and 1C). Unexpectedly, HBV infection did not affect the proliferation of HLCZ01 cells (Figure 1D). Cytoskeletal reorganization is characterized with the epithelial-mesenchymal transition (EMT) of cancer.<sup>25</sup> Here, cytoskeleton changes represented by lamellipodia and stress fibers in HLCZ01 cells were increased by the infection of HBV (Figure 1E). Meanwhile, migratory ability of HLCZ01 cells was enhanced by HBV infection (Figure S1). Thus, HBV infection enhances PD-L1 expression and cancer phenotypes in hepatic cancer cells. Consistent with the influence on cell proliferation, HBV infection had no influence on the growth of tumors formed by HLCZ01 cells in immune-deficient NOD CRISPR *Prkdc Il2r gamma* (NCG) mice (Figure 1F). Considering for the oncogenic role of HBV, we speculated that HBV infection may not only affect the malignant phenotypes of hepatic cancer cells, but also promote the development and progression of HCC by regulating the immune microenvironment. Meanwhile, the remarkable cancer phenotypes and slow tumor-formation post HBV infection reveal the application potential of HLCZ01 cells for studying HBV-associated HCC.

Our previous studies uncovered that ISG12a enhances the innate immune response and promotes cancer immunity,<sup>20,21</sup> exerting antiviral, and anticancer effects. Meanwhile, the results of RNA sequence in our previous study uncovered that ISG12a may regulate PI3K-AKT signaling pathway.<sup>21</sup> ISG12a, ISG12b, and ISG12c together form the ISG12 gene family. Interestingly, only ISG12a was found with responsive effect to IFN treatment in hepatic cancer cells (Figure S2), consisting with the previous report.<sup>26</sup> The responsive effect of ISG12a to IFN treatment presents a potential strategy for therapeutically HCC. With HBV infection, PD-L1 level was upregulated on HLCZ01 cells (Figures 1B and 1C), but ISG12a level in cell lysates was simultaneously downregulated (Figure 2A). To determine the regulatory effect of ISG12a on HBV-associated HCC, HBV-infected HLCZ01 cells was infected with lentivirus (LT) to silence ISG12a expression. Compared with that of negative control LT-shCtrl, silencing ISG12a (LT-shISG12a) not only increased PD-L1 level on HBV-infected HLCZ01 cells as well as p-AKT and p-mTOR levels in cell lysates (Figures 2B–2D), but also promoted the proliferation and cytoskeleton changes represented by lamellipodia and stress fibers (Figures 2E and 2F). Notably, the increased levels of PD-L1, p-AKT, and p-mTOR in ISG12a-silenced of HBV-infected HLCZ01 cells was decreased by the overexpression of ISG12a (Figure 2G). Moreover, lamellipodia and stress fibers were also decreased in HBV-infected HLC01 cells with the forced expression of ISG12a (Figure 2H), and the levels of HBcAg and HBsAg and nuclei acid levels of HBV pgRNA and DNA in HBV-infected HLCZ01 cells were all downregulated with the upregulation of ISG12a (Figures 2I and S3). All these findings suggested the anticancer and anti-HBV effects of ISG12a.

### High level of ISG12a may improve the overall prognosis and promote the anticancer effect of NK cells in HBV-associated HCC

To evaluate the clinical significance of ISG12a in cancer research, we evaluated the transcriptomes of HCC in the Cancer Genome Atlas (TCGA) database. It turned out that the level of *ISG12a* transcript in cancerous tissues (CAs) with HBV infection was significantly lower than that in para-cancerous tissues (*para*-CAs) and that in CAs without HBV or HCV infection (Figures 3A and 3B; Table S1). Notably, HCC cases with high level of *ISG12a* transcript was mainly concentrated in Stage I and II of China liver cancer staging (CNLC), and vice versa (Figure 3C). Thus, low expression of ISG12a may lead to vascular invasion or extrahepatic metastasis of HCC accompanying with poor liver function and terrible physical condition. Moreover, high level of *ISG12a* in CAs brought a nearly 20% advantage in 5-year overall survival rate ( $p = 0.0230$ ) for HBV-associated HCC (Figure 3D). By companion, *ISG12a* level exhibited no significant influence on 5-year overall survival

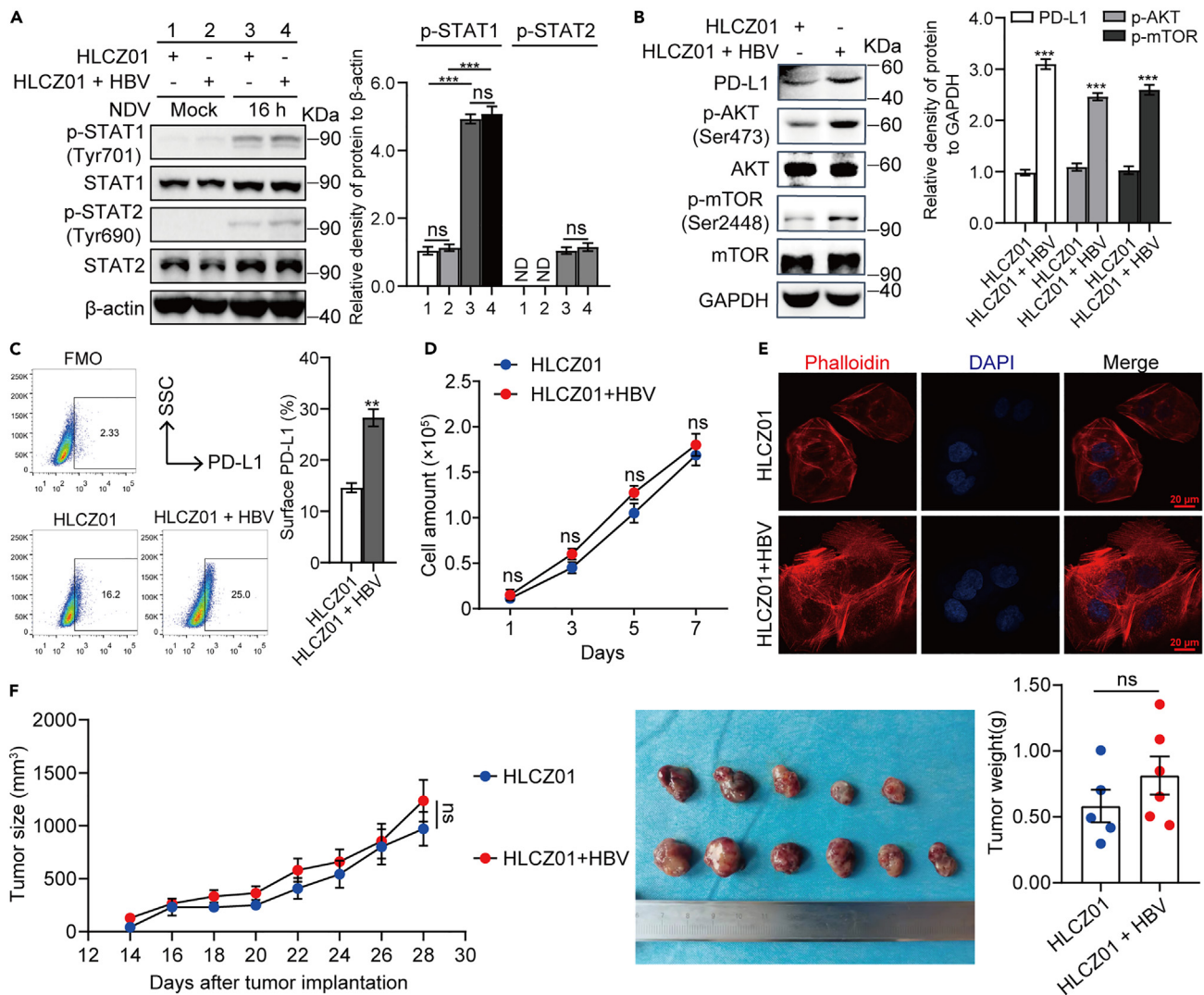


**Figure 1. Influence of HBV infection on malignant phenotypes of HLCZ01 cells**

(A) Immunoblots for p-STAT1, STAT1, p-STAT2, STAT2 levels in lysates of HLCZ01 cells with or without HBV infection. Cells were infected with NDV for 16 h, and the multiplicity of infection (MOI) of NDV was 0.2. ND, not detected.

(B) Immunoblots for PD-L1, p-AKT, AKT, p-mTOR, and mTOR levels in lysates of HLCZ01 cells with or without HBV infection.

(C) Flow cytometry analysis for surface PD-L1 level on HLCZ01 cells with or without HBV infection.

(D) Proliferation of HLCZ01 cells with or without HBV infection. Cell proliferation was determined by counting using a blood counting chamber.

(E) Immunofluorescence staining for F-actin level in HLCZ01 cells with or without HBV infection. Magnification: 600 $\times$ , and scale bar: 20  $\mu$ m.

(F) Tumor formation of HLCZ01 cells with or without HBV infection in NCG mice (n = 5 or 6). Minimum scale of the ruler: 1 mm.

Experiments were independently replicated at least two times with similar results. Data were analyzed by one-way ANOVA (A) or unpaired two-sided Student's t tests (B–D and F), and are presented as mean  $\pm$  SEM with three replicate experiments (A and B) or at least three biological replicates (C, D, and F). \*\*p < 0.01 and \*\*\*p < 0.001.

rate of HCC without HBV or HCV infection (p = 0.5406) (Figure 3E). Thus, high level of ISG12a may predict a promising prognosis for HBV-associated HCC.

Our previous research found that ISG12a may promote the anticancer immunity of NK cells,<sup>21</sup> but direct evidence between ISG12a regulation and NK cell signatures in HBV-associated HCC and *in vivo* study are lacking. Herein, Pearson correlation analyses revealed a similar expression profile between ISG12a and NK cell signatures with active phenotypes including NCR3 (r = 0.4718, p = 0.0003, n = 55), HCST (r = 0.4420, p = 0.0007, n = 55), 2B4 (r = 0.5177, p < 0.0001, n = 55), PRF1 (r = 0.4976, p = 0.0001, n = 55), and GZMA (r = 0.5232, p < 0.0001, n = 55) in CAs of HBV-associated HCC (Figure 3F). It seems that high expression of ISG12a might indicate the presence of active NK cells in HBV-associated HCC. We further conducted *in vivo* experiments to determine our speculation. It turned out that the growth rate and weight of tumors formed by HBV-infected HLCZ01 cells as well as the HBsAg level in plasma of NCG mice were increased with ISG12a

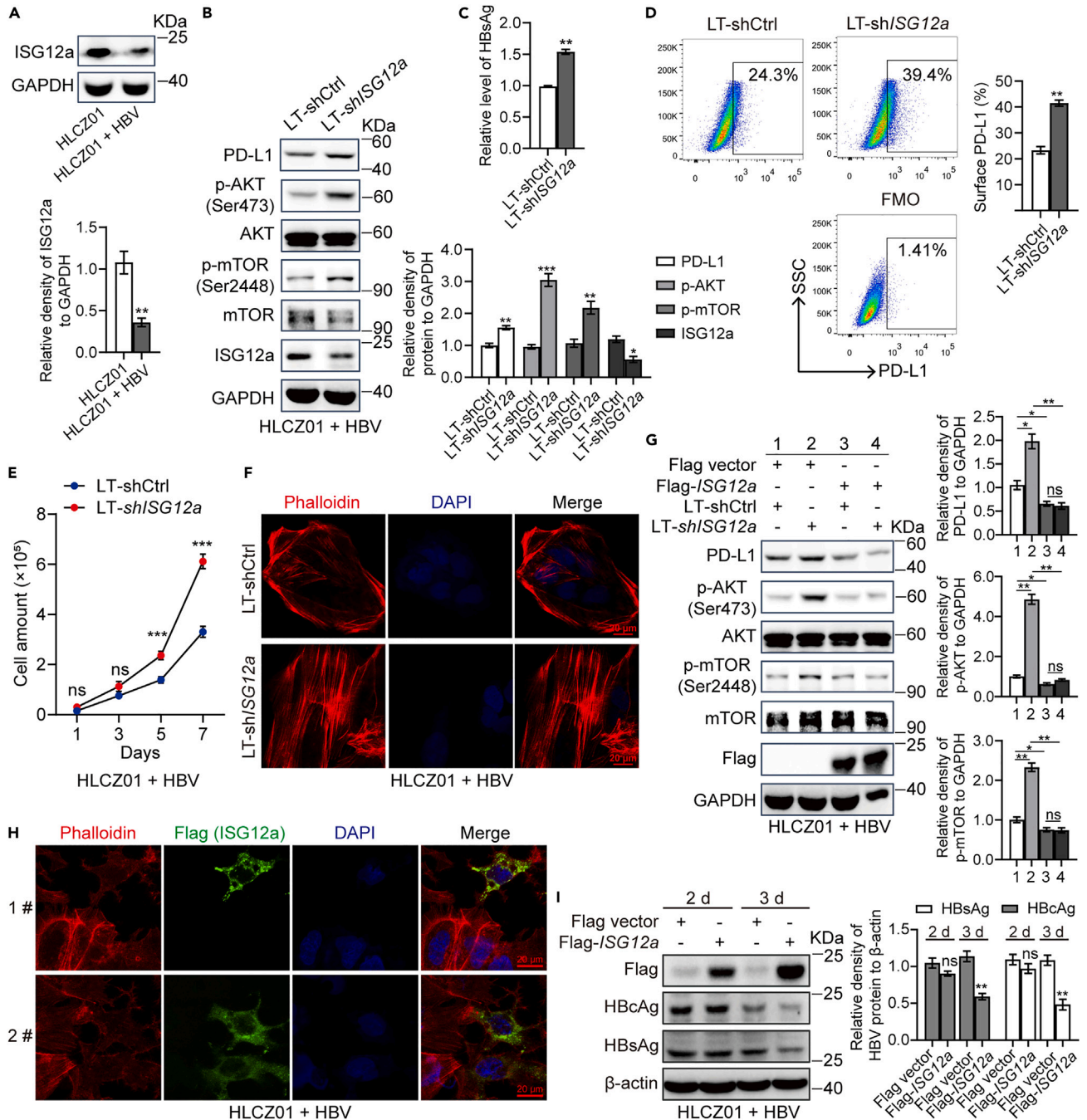


**Figure 2. Inhibitory effect of ISG12a on PD-L1 expression and cancer phenotypes of HBV-infected HLCZ01 cells**

(A) Immunoblots for ISG12a level in HLCZ01 cells with or without HBV infection.  
 (B) Immunoblots for PD-L1, p-AKT, AKT, p-mTOR, mTOR, and ISG12a levels in lysates of HBV-infected HLCZ01 cells with ISG12a knockdown.  
 (C) ELISA for HBsAg level in supernatants of HBV-infected HLCZ01 cells with ISG12a knockdown.  
 (D) Flow cytometry analysis for surface PD-L1 level on HBV-infected HLCZ01 cells with ISG12a knockdown.  
 (E) Proliferation of HBV-infected HLCZ01 cells with ISG12a knockdown. Cell proliferation was determined by counting using a blood counting chamber.  
 (F) Immunofluorescence staining for F-actin level in HBV-infected HLCZ01 cells with ISG12a knockdown. Magnification: 600 $\times$ , and scale bar: 20  $\mu$ m.  
 (G) Immunoblots for PD-L1, p-AKT, AKT, p-mTOR, mTOR, and Flag levels in HBV-infected HLCZ01 cells. The stably infected cells using lentivirus for silencing ISG12a expression were transfected with vector control or Flag-*ISG12a* plasmid for 72 h.  
 (H) Immunofluorescence staining for F-actin level in HBV-infected HLCZ01 cells with the overexpression of ISG12a. Magnification: 600 $\times$ , and scale bar: 20  $\mu$ m.

**Figure 2. Continued**

(I) Immunoblots for Flag, HBcAg, and HBsAg levels in lysates of HBV-infected HLCZ01 cells. Cells were transfected with control vector or Flag-ISG12a plasmid for 2 or 3 days (d).

Experiments were independently replicated at least two times with similar results. Data were analyzed by unpaired two-sided Student's *t* tests (A–E and I) or one-way ANOVA (G), and are presented as mean  $\pm$  SEM with three replicate experiments (A, B, G, and I) or at least three biological replicates (C–E). \**p* < 0.05, \*\**p* < 0.01 and \*\*\**p* < 0.001.

knockdown (Figures 4A–4D). Notably, the wild-type NK-92 cells exhibited promising effect on suppressing tumor growth and HBV replication, especially for that in ISG12a-silenced group (Figures 4A–4D). The immunohistochemistry (IHC) staining of CD56 suggested the infiltrations of NK cells in mice tumors (Figure S4). Moreover, the mouse weight was almost unchanged in experiments (Figure 4E), and the survival rates of NCG mouse were significantly improved by NK cell treatment (Figure 4F). These data suggested that tumor intrinsic ISG12a may promote the anticancer effect of NK cells in HBV-associated HCC.

**ISG12a inhibits PD-L1 expression in HBV-infected hepatic cancer cells by regulating the TRIM21-AKT- $\beta$ -catenin signal axis**

The previous study suggested that AKT may involve in regulatory effect of ISG12a on anticancer effect of NK cells by regulating PD-L1 expression. In fact, the upregulated levels of PD-L1 and HBsAg by AKT was indeed lowered by ISG12a in HBV-infected HLCZ01 cells (Figures 5A and 5B), and similar regulation of ISG12a and AKT on PD-L1 expression was also observed in Huh7 cells (Figure S5A). Lysine 63 (K63)-dependent ubiquitination of AKT promotes its phosphorylation activation.<sup>27</sup> However, the protein structure of ISG12a determines its inability in direct regulation on AKT ubiquitination. Interestingly, results of protein mass spectrometry presented the potential interaction between E3 ubiquitin ligase TRIM21 and ISG12a (Table S2). Meanwhile, our previous study reported that TRIM21 enhances the innate immune response to viral infection,<sup>28</sup> and TRIM21-ISG12a interaction mediates cell pyroptosis in viral infection.<sup>22</sup> Herein, the inhibitory effect of ISG12a and TRIM21 on *p*-AKT and PD-L1 was observed in HBV-infected HLCZ01 cells and HepG2.2.15 cells (Figures 5C and 5D). Notably, the suppression of ISG12a on K63-dependent ubiquitin modification of AKT was enhanced by TRIM21 in HBV-infected HLCZ01 and HEK293T cells (Figures 5E and S5B), and Pearson correlation analysis revealed a similar expression profile between the transcript levels of ISG12a and TRIM21 in CAs of HBV-associated HCC ( $r = 0.5864$ ,  $p < 0.0001$ ,  $n = 55$ ) (Figure S5C). Excepting for TRIM21-AKT interaction, ISG12a-AKT interaction was only observed in HBV-infected HLCZ01 cells while not in HEK293T cells (Figures 5E and S5B), indicating the high activity of ISG12a in suppressing HBV-associated HCC. Moreover, HBV replication in HLCZ01 cells was limited by ISG12a and TRIM21 as well as the treatment of NK-92 cells (Figure 5F). Thus, tumor intrinsic ISG12a and PD-1 deficient NK cells together restrict HBV-associated tumor growth and HBV replication. However, the presence of PD-1 may limit the anticancer and anti-HBV effects of NK cells by interacting with PD-L1 on hepatic cancer cells.

In the classical Wnt/ $\beta$ -catenin signaling pathway, CK1 $\alpha$  first phosphorylates  $\beta$ -catenin at Ser45, and then GSK-3 $\beta$  phosphorylates  $\beta$ -catenin at Ser33, Ser37, and Thr41, resulting in the ubiquitin degradation of  $\beta$ -catenin.<sup>21,29</sup> However, AKT can phosphorylates  $\beta$ -catenin at Ser552, resulting in a nuclear-localized activation of  $\beta$ -catenin,<sup>29,30</sup> thereby promoting PD-L1 expression.<sup>31</sup> Herein, the translocation of *p*- $\beta$ -catenin (Ser552) in nuclei of HBV-infected HLCZ01 cells was enhanced with the knockdown of ISG12a (Figure 6A), and PD-L1 expression that regulated by AKT was turned out to be dependent on *p*- $\beta$ -catenin level (Figure 6B), suggesting the potential regulation of ISG12a on AKT- $\beta$ -catenin signal transduction. In fact, *p*- $\beta$ -catenin level in HBV-infected cells was decreased by both ISG12a and TRIM21 while increased by AKT (Figures 5A, 5C, and 5D). Moreover, PD-L1 level in cell lysates and HBsAg level in supernatants of HBV-infected HLCZ01 cells were both upregulated by the wild-type and phosphorylated activated mutant S552D of  $\beta$ -catenin (Figures 6C–6E). Meanwhile, the upregulated PD-L1 level and HBV replication by  $\beta$ -catenin was decreased by the forced expression of ISG12a (Figures 6C–6E). However, PD-L1 level in wild-type HLCZ01 cells was almost unaffected by the wild-type  $\beta$ -catenin and the mutant S552D (Figure S5D), indicating the specific regulation of *p*- $\beta$ -catenin in HBV-associated HCC. Notably, the transcriptional activity of *PD-L1* promoter that transfected into HBV-infected HLCZ01 cells was significantly upregulated by Flag-CTNNB1a and Flag-S552D (Figure 6F), indicating that *p*- $\beta$ -catenin (Ser552) may be a transcription factor of *PD-L1* gene. Actually, our previous study uncovered that  $\beta$ -catenin binds to the *PD-L1* promoter in the regions –837 bp to –636 bp and –493 bp to –393 bp, promoting the transcriptional activity of *PD-L1* gene.<sup>21</sup> Through conducting ChIP assays, we determined the role of  $\beta$ -catenin as a transcription factor of *PD-L1* gene in HBV-infected HLCZ01 cells (Figure 6G). These findings suggested that ISG12a may inhibit *PD-L1* expression through suppressing the phosphorylation modification of  $\beta$ -catenin at Ser552 in HBV-infected hepatic cancer cells. Though regulating the TRIM21-AKT- $\beta$ -catenin signal axis, ISG12a inhibits *PD-L1* expression in HBV-associated HCC.

**Blockades of PD-1 and PD-L1 enhance the anticancer effect of NK cells toward HBV-associated HCC caused by the low expression of ISG12a**

Next, the application potential of PD-1/PD-L1 blockades in NK cell mediated immunotherapy toward HBV-associated HCC with low level of ISG12a was evaluated. For this purpose, PD-1 was exogenously expressed in NK-92 cells by LT (Figure 7A), and the results of flow cytometry suggested the high level of PD-1 protein on surface of LT-infected NK-92 cells (Figure 7B). Aforementioned study found that the suppression of wild-type NK-92 cells on growth of tumor formed by HBV-infected HLCZ01 cells was independent of ISG12a expression (Figure 4). However, the exogenous expression of PD-1 on NK-92 cells might cause immune evasion of hepatic cancer cells, inhibiting the immune surveillance of NK cells by activating PD-1/PD-L1 signaling in HBV-associated HCC. In fact, significant differences about the size and weight of tumors formed by HBV-infected HLCZ01 cells were observed between LT-shCtrl and LT-shISG12a groups under the treatment of IgGs (Figures 7C and 7D). Thus, the immunosuppressive PD-1/PD-L1 signaling caused by the downregulated ISG12a level in cancer cells limits

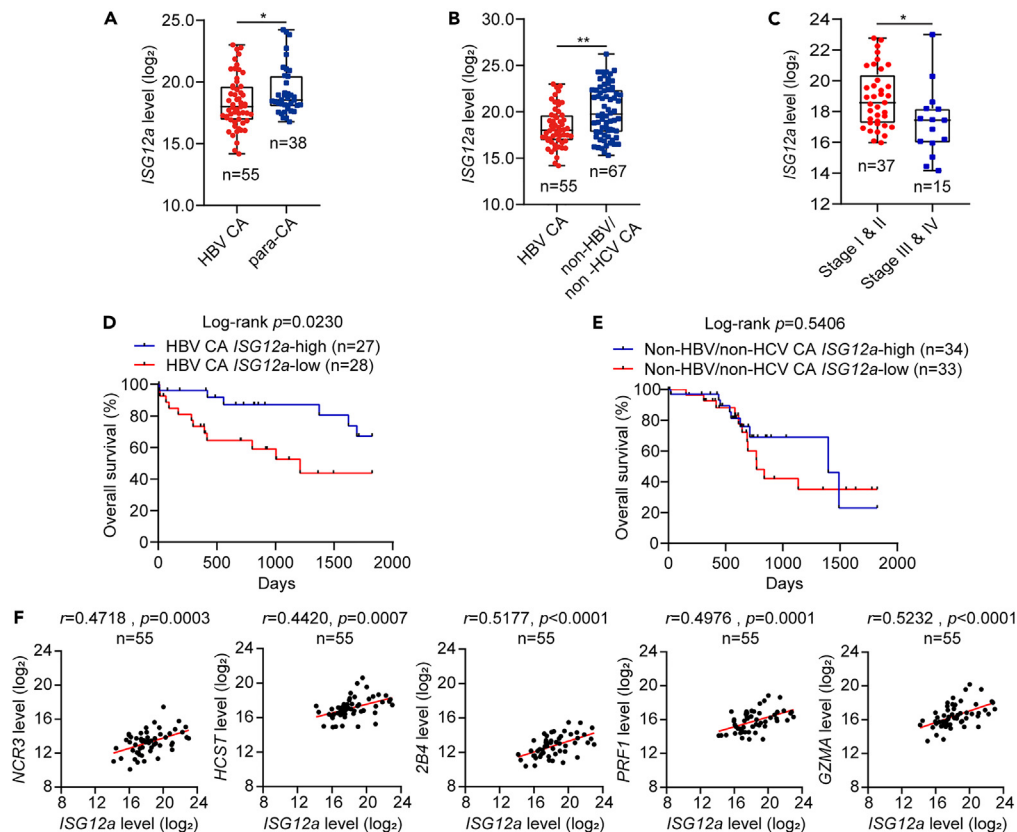


**Figure 3. Influence of tumor intrinsic ISG12a on prognosis and NK cell activation in HBV-associated HCC**

(A) Scatterplot showing the transcript level of *ISG12a* in HBV-infected CAs (n = 55) and *para*-CAs (n = 38) in TCGA database. Detailed information of HCC samples is listed in [Table S1](#).

(B) Scatterplot showing the transcript level of *ISG12a* in HBV-infected CAs (n = 55) and non-HBV/non-HCV-infected CAs (n = 67) in TCGA database.

(C) Scatterplot showing the transcript level of *ISG12a* in Stages I & II (n = 37) and III & IV (n = 15).

(D) Kaplan-Meier analyses for 5-year overall survival rate of HCC with HBV infection presenting high (n = 27) and low (n = 28) levels of *ISG12a* in CAs, as analyzed by log rank test.

(E) Kaplan-Meier analyses for 5-year overall survival rate of HCC without HBV or HCV infection presenting high (n = 34) and low (n = 33) levels of *ISG12a* in CAs, as analyzed by log rank test.

(F) Pearson's correlation coefficients for the transcript level of *ISG12a* and active NK cell signatures (*NCR3*, *HCST*, *2B4*, *PRF1*, and *GZMA*) in CAs of HBV-associated HCC. n = 55.

Data were analyzed by unpaired two-sided Student's t tests, and are presented as mean  $\pm$  SEM (A–C). Significance levels: \*p < 0.05 and \*\*p < 0.01.

the anticancer effect of NK cells that equipped with PD-1 expression. By comparison, treatments of ICBs including PD-L1 inhibitor atezolizumab and PD-1 inhibitor nivolumab both enhanced the therapeutic efficacy of NK cells in HBV-associated HCC, eliminating the difference of tumor growth caused by silencing *ISG12a* ([Figures 7C](#) and [7D](#)). Meanwhile, the body weight of mice was also unchanged in experiments ([Figures 7E](#) and [7F](#)). Thus, disrupting PD-1/PD-L1 signaling caused by the low expression of *ISG12a* using ICBs may improve the anticancer effect of NK cells toward HBV-associated HCC.

## DISCUSSION

Due to the preference for species and tissues, HBV related research has been limited for the lack of cell and animal models.<sup>32,33</sup> Huh7 and HepG2 cells as well as HepG2.2.15, HepaRG, and HepG2-NTCP cells that derived from HepG2 cells have defects either in infection and invasion of HBV or *in vitro* cultivation.<sup>34</sup> Human HCC cell line HLCZ01 has similar morphology and function with the primary hepatocytes and supports the complete life cycle of HBV,<sup>24</sup> being a promising alternative for HBV-related research. Through examining proliferation and cytoskeleton changes represented by lamellipodia and stress fibers, this study approved the oncogenic role of HBV and identified the potential suppression of tumor intrinsic *ISG12a* on HBV-associated HCC. The increased cancer phenotypes including lamellipodia and stress fibers and upregulated proliferation of HBV-infected HLCZ01 cells with *ISG12a* knockdown indicated the potential inhibition of *ISG12a* on malignant transformation of HBV-associated HCC. The further study based on TCGA database figured out the role of *ISG12a* as a malignant transformation regulator and a prognostic factor in HBV-associated HCC, which may be mechanically explained by the upregulated *p*-AKT, *p*-mTOR,

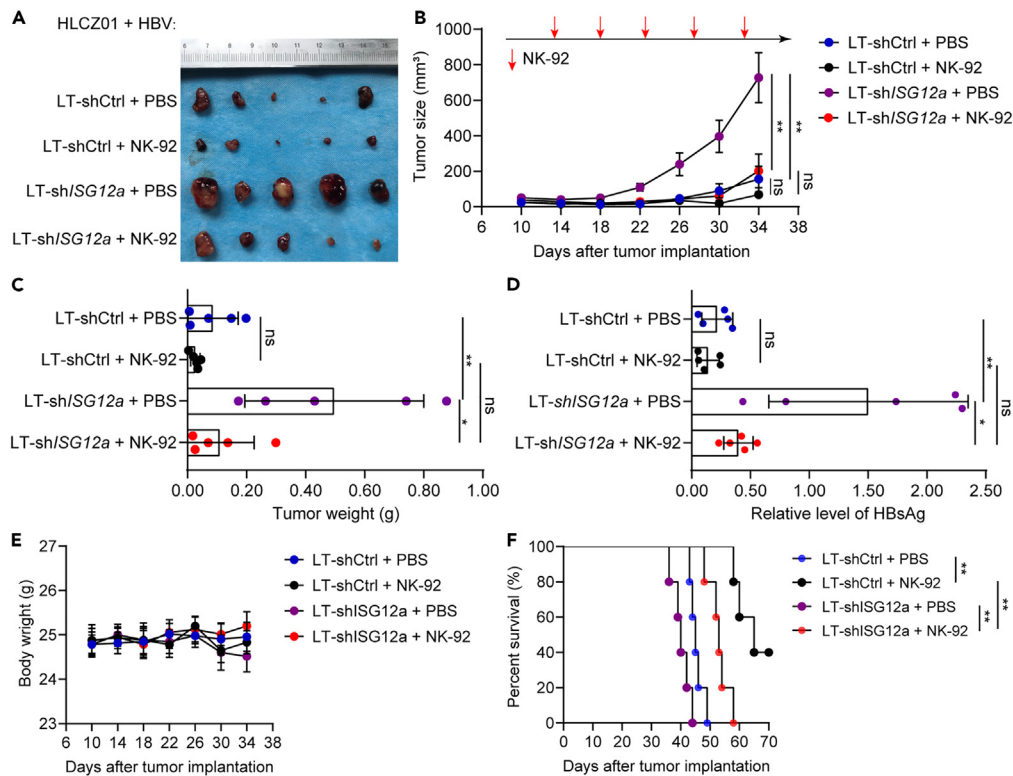


**Figure 4. Inhibitory effect of ISG12a and NK cells on HBV-associated HCC**

(A–C) Image, growth curve, and weight of formed tumors in NCG mice within 34 days after subcutaneous injection of HBV-infected HLCZ01 cells with ISG12a knockdown ( $n = 5$ ).  $5.0 \times 10^6$  wild-type NK-92 cells in sterile PBS accompanying with 2000 U rhIL-2 were administrated into mouse by intraperitoneal injection at the indicated time points in red arrows. Minimum scale of the ruler: 1 mm.

(D) ELISA for HBsAg level in plasma of tumor formed mice in (A).

(E) Statistical analysis for the weight of mice in (A).

(F) Kaplan-Meier analysis for the survival rate of mice in (A) within 70 days.

Experiments were independently replicated two times. Data were analyzed by one-way ANOVA, and are presented as mean  $\pm$  SEM with five biological replicates (B–D). \* $p < 0.05$  and \*\* $p < 0.01$ .

and PD-L1 levels.<sup>35,36</sup> Furthermore, administration of wild-type NK-92 cells in NCG mice dramatically suppressed the growth of tumors formed by ISG12a-silenced of HBV-infected HLCZ01 cells. Actually, the depressed cytolytic activity and reduced number of NK cells are indicators of malignant transformation and poor prognosis of HCC.<sup>37,38</sup> Therefore, tumor intrinsic ISG12a exerts tumor suppressor role in HBV-associated HCC. Meanwhile, the antigen levels of HBcAg and HBsAg and the nuclei acid levels of HBV pgRNA and DNA in HBV-infected HLCZ01 cells were downregulated by the high level of ISG12a, indicating the anti-HBV effect of ISG12a. However, it may be due to the high stability of cccDNA, ISG12a exhibits limited effect on decreasing cccDNA level in cell culture.

With the development and progression of HBV-associated HCC, CD8<sup>+</sup> T cells are dysfunctional and exhausted, which are characterized with high PD-1 expression, low IFN- $\gamma$  and TNF secretion, and prone apoptosis.<sup>39,40</sup> Blockades of PD-1 and PD-L1 may reverse CD8<sup>+</sup> T cell dysfunction and disrupt HBV persistence, but the risk of graft-versus-host disease, cytokine release syndrome, and neurotoxicity of T cell base immunotherapy may limit the clinic application.<sup>41,42</sup> By comparison, the relatively high safety and high feasibility of the “off-the-shelf” manufacturing as well as the extensive source make NK cell therapy a new focus in cancer immunotherapy.<sup>43</sup> NK cells account for only 5–15% of lymphocytes in peripheral blood of healthy individuals, but approximately 90% of circulating NK cells are CD56<sup>dim</sup> cells that are equipped with a strong cytolytic function toward cancer cells and viral-infected cells.<sup>44,45</sup> This study presented the significant Pearson’s correlation coefficients between the expression profiles of ISG12a and active NK cell signatures in CAs of HBV-associated HCC, providing evidence for the potential regulation of tumor intrinsic ISG12a on NK cell activation. Moreover, the inhibitory effect of PD-1-deficient NK-92 cells on growth of tumors formed by HBV-infected HLCZ01 cells in NCG mice was independent of ISG12a expression, suggesting the high efficacy of NK cells in suppressing HBV-associated HCC. Meanwhile, ISG12a and TRIM21 in hepatic cancer cells and PD-1-deficient NK-92 cells exhibited excellent effect on inhibiting HBV replication. In fact, HBV promotes PD-L1 expression on cancer cells in our study, which was also approved by other studies.<sup>46,47</sup> PD-1/PD-L1 signaling mediates the exhaustion of NK cells and the immune evasion of cancer cells.<sup>48</sup> Thus, PD-1/PD-L1 signaling may play an important role in suppressing the anticancer and anti-HBV effects of NK cells in HBV-associated HCC. For this reason, under the treatment of IgGs, the anticancer effects of PD-1-expressed NK-92 cells toward ISG12a-silenced HBV-infected HLCZ01 cells were greatly

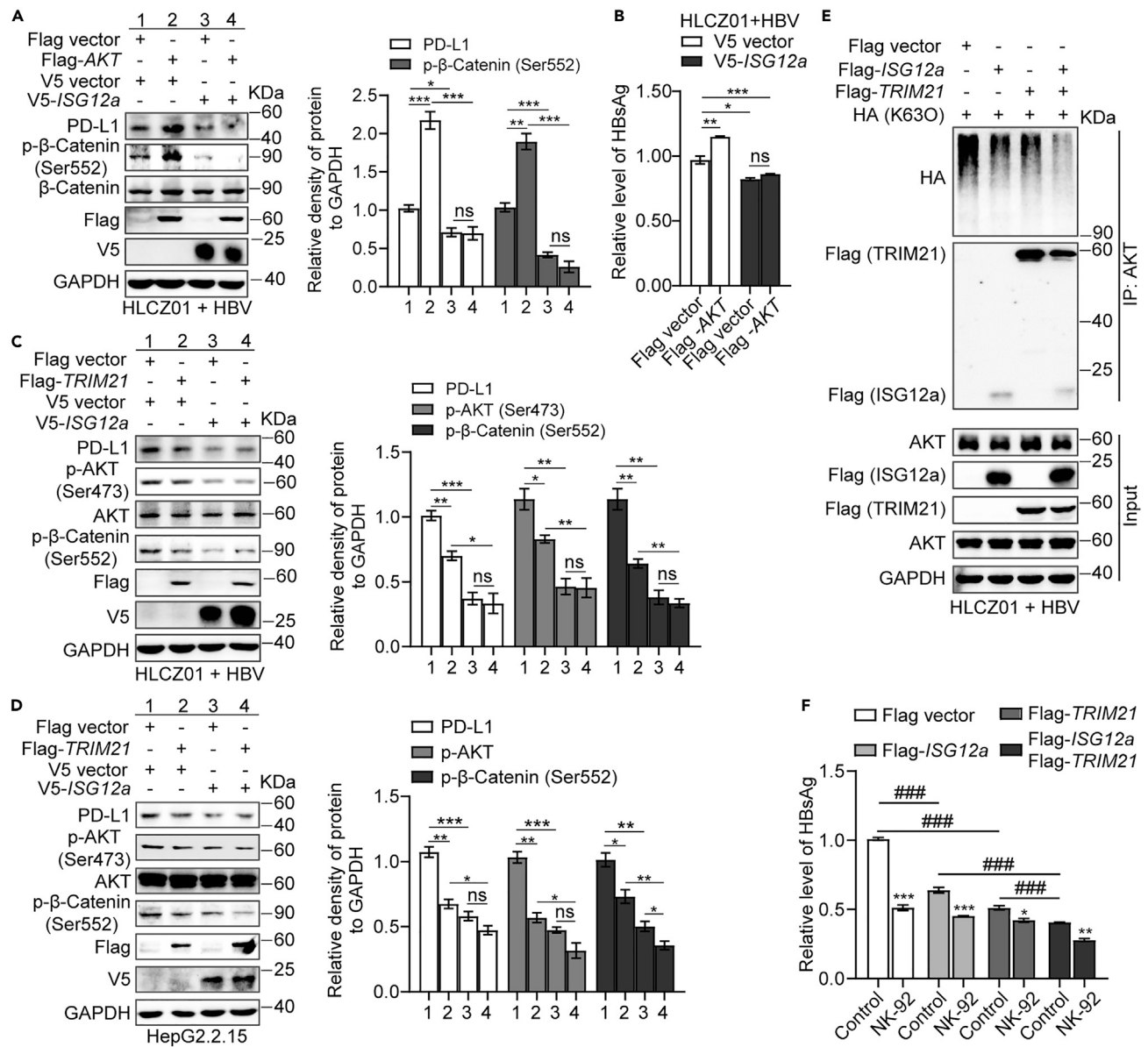


**Figure 5. Regulatory effect of ISG12a-TRIM21-AKT-β-catenin signal axis on PD-L1 expression in HBV-infected HLCZ01 cells**

(A and B) Immunoblots for PD-L1, p-β-catenin, β-catenin, Flag, and V5 levels in lysates (A) and ELISA for relative HBsAg level in supernatants (B) of HBV-infected HLCZ01 cells with the overexpression of ISG12a and AKT for 72 h.

(C and D) Immunoblots for PD-L1, p-AKT, AKT, p-β-catenin, β-catenin, Flag, and V5 levels in lysates of persistent HBV-infected HLCZ01 cells (C) or HepG2.2.15 cells (D) with the overexpression of ISG12a and TRIM21 for 72 h.

(E) Co-IP for K63-modified ubiquitin levels of AKT and TRIM21-AKT-ISG12a interactions in HBV-infected HLCZ01 cells. Cell lysates were immunoprecipitated with an anti-AKT antibody and examined for HA and Flag by immunoblots.

(F) ELISA for relative HBsAg level in supernatants of HBV-infected HLCZ01 cells. After transfection with control vector or plasmids with ISG12a and TRIM21 expression for 24 h, cells were cocultured with the wild-type NK-92 cells (E:T = 2:1) for 48 h.

Experiments were independently replicated at least two times with similar results. Data were analyzed by unpaired one-way ANOVA, and are presented as mean ± SEM with at least three biological replicates (B and F) or three replicate experiments (A, C, and D). \*p < 0.05, \*\*p < 0.01, and \*\*\*, ###p < 0.001.

suppressed. Therefore, inhibiting PD-L1 expression by ISG12a in HBV-infected hepatic cancer cells is an important factor for maintaining the immune surveillance of NK cells. Excepting for direct cytolytic function, NK cells also secrete cytokines for recruiting DCs and T cells to promote cancer immune control,<sup>49</sup> and NK cell frequency defines the response efficiency of immune checkpoints in tumor microenvironments.<sup>50</sup> These advantages determine the high efficacy of NK cell therapy in HBV-associated HCC.

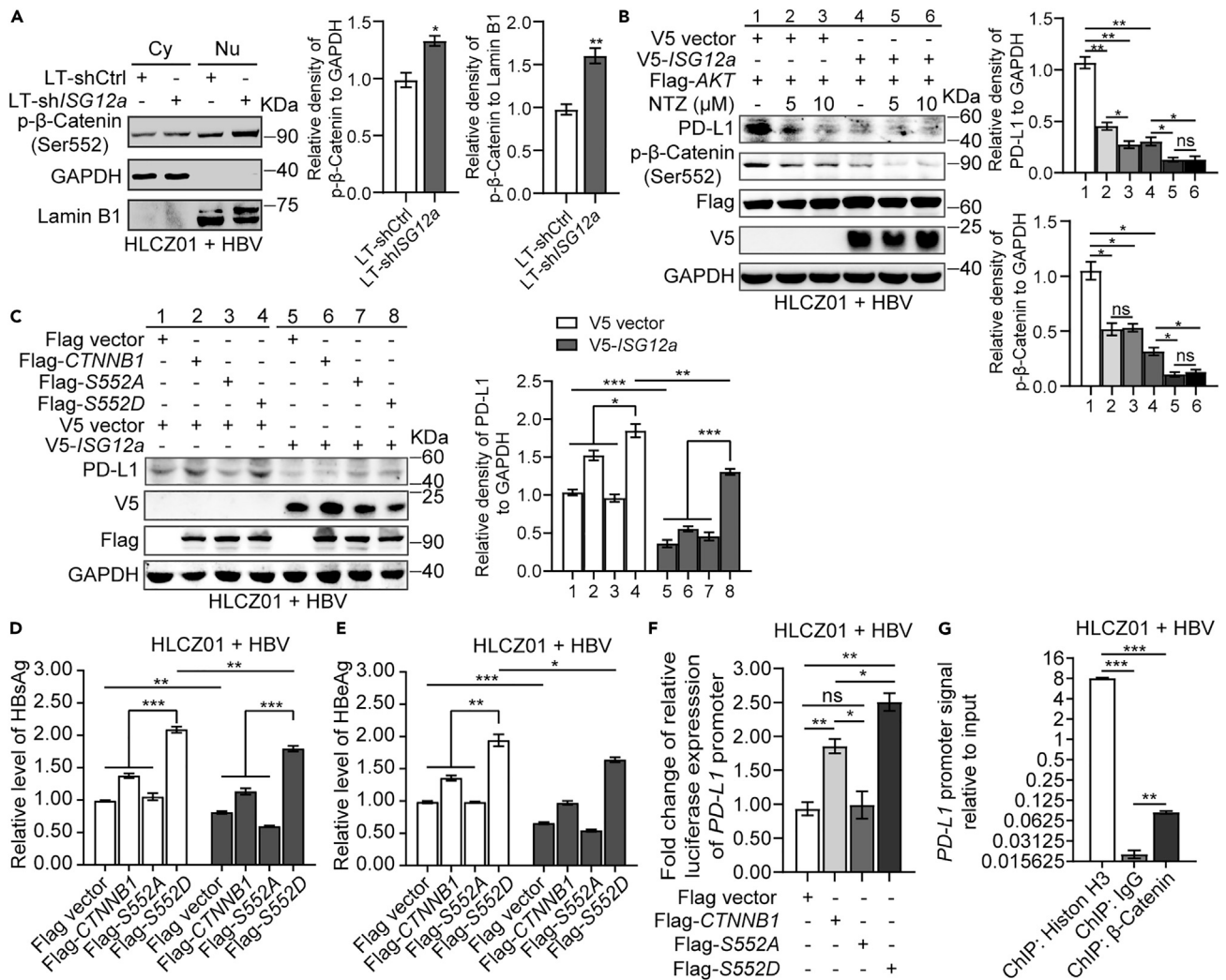


**Figure 6. Regulatory effect of ISG12a on AKT-β-catenin signal transduction in HBV-infected HLCZ01 cells**

(A) Immunoblots for p-β-catenin level in cytoplasm (Cy) and nuclei (Nu) of HBV-infected HLCZ01 cells with the knockdown of ISG12a.

(B) Immunoblots for p-β-catenin level in HBV-infected HLCZ01 cells. Cells were transfected with Flag-AKT plasmid and V5-ISG12a plasmid or control vector for 72 h, which were further treated with vehicle DMSO or NTZ for 12 h.

(C–E) Immunoblots for PD-L1, V5, and Flag levels in lysates of HBV-infected HLCZ01 cells with forced expression of ISG12a and wild type (Flag-CTNNB1) or mutated (Flag-S552A and Flag-S552D) β-catenin for 72 h.

(F) Fold change of luciferase expression of PD-L1 promoter in HBV-infected HLCZ01 cells with the forced expression of wild type (Flag-CTNNB1) and mutants (Flag-S552A and Flag-S552D) of β-catenin for 36 h.

(G) qRT-PCR showing interaction of PD-L1 promoter fragment with β-catenin protein in HBV-infected HLCZ01 cells, as determined by ChIP assay.

Experiments were independently replicated at least two times with similar results. Data were analyzed by unpaired two-sided Student's t tests (A) or one-way ANOVA (B–G), and are presented as mean ± SEM with three replicate experiments (A–C) or three biological replicates (D–G). \*p < 0.05, \*\*p < 0.01, and \*\*\*p < 0.001.

PD-1 expressed on NK cells with activation and response phenotypes may bind to PD-L1 expressed on cancer cells, causing immune evasion of cancer cells from immune surveillance of NK cells.<sup>48,51</sup> PD-1 or PD-L1 monotherapy in HCC have been reported with a responsive rate ranged from 15% to 23%, and combination therapies ICBs present an increasing responsive rate to approximately 30%.<sup>52</sup> Although ICBs contribute to immunotherapy mediated by NK cells,<sup>48,53,54</sup> its behind mechanism in HBV-associated HCC is unclear. In HBV-associated HCC, treatments of atezolizumab and nivolumab reversed the immunosuppressive PD-1/PD-L1 signaling on NK cells in the background of low expression of tumor intrinsic ISG12a, presenting promising choices for improving the immunotherapeutic efficacy of NK cells.

In conclusion, tumor intrinsic ISG12a promotes the anticancer effect of NK cells in HBV-associated HCC through regulating PD-1/PD-L1 signal transduction. This study reveals the regulatory effect of tumor intrinsic ISG12a on NK cell activity in development and progression of HBV-associated HCC, underlining the necessity of innate immunity in supporting anticancer and antiviral immunity. These findings may provide

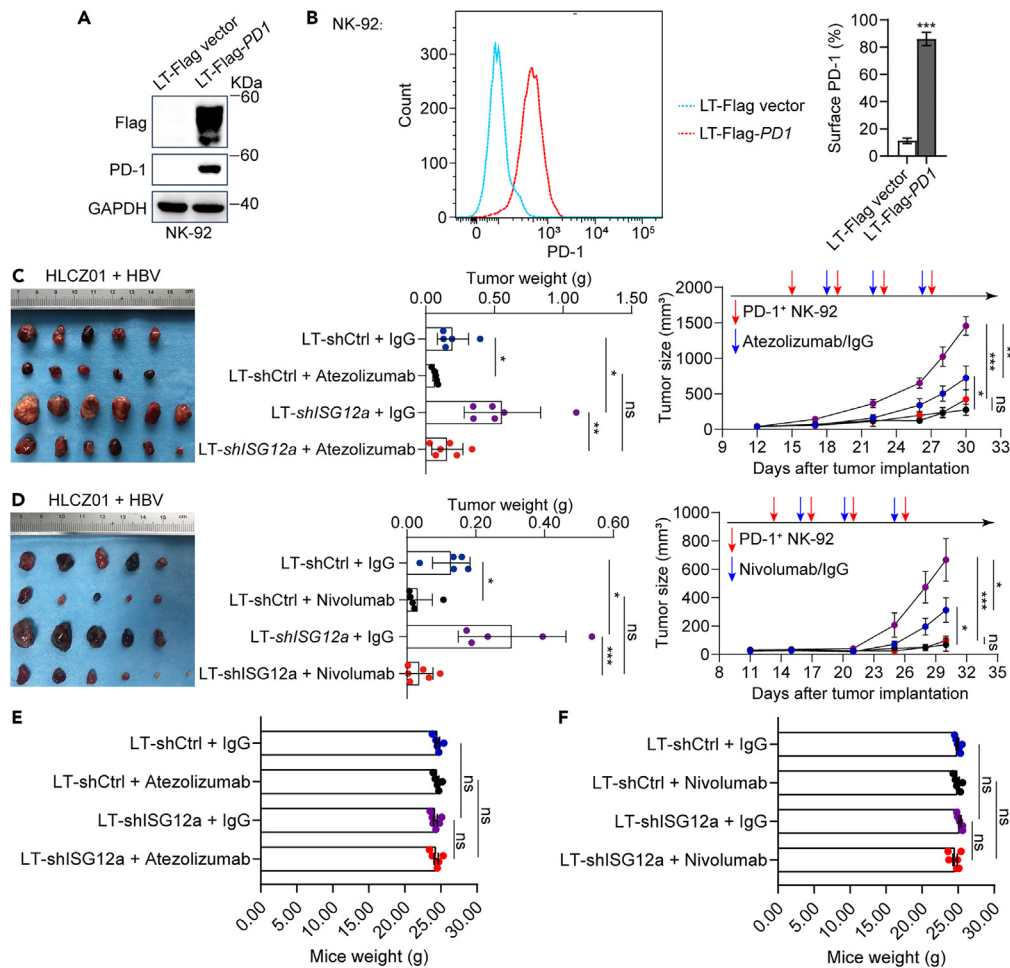


**Figure 7. Application potential of PD-1 and PD-L1 blockades in immunotherapy mediated by NK cells toward HBV-associated HCC with low expression of ISG12a**

(A) Immunoblots for Flag and PD-1 levels in lysates of NK-92 cells. NK-92 cells were stably infected with lentivirus to overexpress PD-1.

(B) Flow cytometry for surface PD-1 level on NK-92 cells. NK-92 cells were stably infected with lentivirus to overexpress PD-1.

(C and D) The formed tumors of HBV-infected HLCZ01 cells with ISG12a knockdown in NCG mice at 30 days ( $n = 5$  or  $6$ ).  $5.0 \times 10^6$  PD-1-overexpressed NK-92 cells accompanying with 2000 U rhIL-2 was administrated into each mouse by intraperitoneal injection at the indicated time points in red arrows, and 200  $\mu$ g of PD-L1 inhibitor atezolizumab (C), PD-1 inhibitor nivolumab (D) or corresponding IgGs was intraperitoneally into mouse at the indicated time points in blue arrows. Minimum scale of the ruler: 1 mm.

Experiments were independently replicated two times with similar results. Data were analyzed by unpaired two-sided Student's *t* tests (B) or one-way ANOVA (C–F), and are presented as mean  $\pm$  SEM with five or six biological replicates. \**p* < 0.05, \*\**p* < 0.01, and \*\*\**p* < 0.001.

sights for improving the therapeutic efficacy of NK cells and ICBs for HBV-associated HCC. Additionally, HLCZ01 is a promising cell model used for conducting HBV-related research, and NK-92 cell line may be a considerable source of NK cell therapy for malignant carcinomas represented by HCC.

### Limitation of the study

The applications of IL-2 deficient NCG mice and CD16-deficient NK-92 cells eliminating the influence of antibody-dependent cell-mediated cytotoxicity (ADCC) in study. Actually, ADCC is an available anticancer mechanism of NK cells,<sup>55</sup> which should be studied in follow-up study. This study mainly reveals that ISG12a promotes the anticancer effect of NK cells, but whether the anticancer effect of ISG12a dependent on the NK cell activation is still need to be explored.

### STAR★METHODS

Detailed methods are provided in the online version of this paper and include the following:

- **KEY RESOURCES TABLE**
- **RESOURCE AVAILABILITY**
  - Lead contact
  - Materials availability
  - Data and code availability
- **EXPERIMENTAL MODEL AND STUDY PARTICIPANT DETAILS**
  - Ethics approval and consent to participate
  - Cell lines
  - Mice
- **METHOD DETAILS**
  - Cell culture
  - Plasmids construction
  - Lentiviral package and infection
  - NDV production
  - Qualitative real-time PCR (qRT-PCR)
  - HBV infection of cell culture
  - Immunoblots and co-immunoprecipitation (co-IP)
  - Immunofluorescence staining
  - Immunohistochemistry (IHC) staining
  - Wound-healing assay
  - Flow cytometry
  - ELISA
  - Dual luciferase reporter assay
  - Chromatin immunoprecipitation (ChIP)
  - HCC in The Cancer Genome Atlas (TCGA) database
  - Xenograft experiment
- **QUANTIFICATION AND STATISTICAL ANALYSIS**

## SUPPLEMENTAL INFORMATION

Supplemental information can be found online at <https://doi.org/10.1016/j.isci.2024.109533>.

## ACKNOWLEDGMENTS

We thank Dr. Chen Liu (Yale University) for providing Huh7 and HepG2.2.15 cells, Dr. Zhengfan Jiang (Peking University) for providing pHA-Ub plasmid, and Dr. Joseph Peiris (University of Hongkong) for providing NDV D817. We thank TCGA database for providing datasets. This work was supported by the National Natural Science Foundation of China (82072269 and 81730064 to H.Z. and 82303190 to R.D.), the National Major Science and Technology Projects of China (2017ZX10202201-005 to H.Z.), the Natural Science Foundation of Hunan Province (2022JJ40110 to R.D.), and the China Postdoctoral Science Foundation (2021M701151 to R.D.).

## AUTHOR CONTRIBUTIONS

R.D. and H.Z. designed research. R.D., R.T., X.L., X.W., and Y.L. performed cell experiments and HBV detection. R.D., R.T., X.L., Y.X., X.W., and B.X. conducted molecular experiments. R.D., R.T., L.W., B.X., D.Y., and X.L. performed animal experiments. R.D., R.T., B.X., and H.Z. contributed to data curation and analyses. R.D. and C.Z. analyzed TCGA database. S.T. and H.Z. supervised the project. R.D. and H.Z. contributed to funding acquisition and wrote the manuscript. All authors have read and agreed to the final manuscript.

## DECLARATION OF INTERESTS

The authors declare no competing interests.

Received: July 20, 2023

Revised: January 16, 2024

Accepted: March 16, 2024

Published: March 19, 2024

REFERENCES

1. Forner, A., Reig, M., and Bruix, J. (2018). Hepatocellular carcinoma. *Lancet* 391, 1301–1314. [https://doi.org/10.1016/S0140-6736\(18\)30010-2](https://doi.org/10.1016/S0140-6736(18)30010-2).
2. Vogel, A., Meyer, T., Sapisochin, G., Salem, R., and Saborowski, A. (2022). Hepatocellular carcinoma. *Lancet* 400, 1345–1362. [https://doi.org/10.1016/S0140-6736\(22\)01200-4](https://doi.org/10.1016/S0140-6736(22)01200-4).
3. Kudo, M., Finn, R.S., Qin, S., Han, K.H., Ikeda, K., Piscaglia, F., Baron, A., Park, J.W., Han, G., Jassem, J., et al. (2018). Lenvatinib versus sorafenib in first-line treatment of patients with unresectable hepatocellular carcinoma: a randomised phase 3 non-inferiority trial. *Lancet* 391, 1163–1173. [https://doi.org/10.1016/S0140-6736\(18\)30207-1](https://doi.org/10.1016/S0140-6736(18)30207-1).
4. Chen, Y., and Tian, Z. (2019). HBV-Induced Immune Imbalance in the Development of HCC. *Front. Immunol.* 10, 2048. <https://doi.org/10.3389/fimmu.2019.02048>.
5. Lee, P.C., Chao, Y., Chen, M.H., Lan, K.H., Lee, I.C., Hou, M.C., and Huang, Y.H. (2020). Risk of HBV reactivation in patients with immune checkpoint inhibitor-treated unresectable hepatocellular carcinoma. *J. Immunother. Cancer* 8, e001072. <https://doi.org/10.1136/jitc-2020-001072>.
6. Itoh, S., Yoshizumi, T., Yugawa, K., Imai, D., Yoshiya, S., Takeishi, K., Toshima, T., Harada, N., Ikegami, T., Soejima, Y., et al. (2020). Impact of Immune Response on Outcomes in Hepatocellular Carcinoma: Association With Vascular Formation. *Hepatology* 72, 1987–1999. <https://doi.org/10.1002/hep.31206>.
7. Gao, Q., Wang, X.Y., Qiu, S.J., Yamato, I., Sho, M., Nakajima, Y., Zhou, J., Li, B.Z., Shi, Y.H., Xiao, Y.S., et al. (2009). Overexpression of PD-L1 significantly associates with tumor aggressiveness and postoperative recurrence in human hepatocellular carcinoma. *Clin. Cancer Res.* 15, 971–979. <https://doi.org/10.1158/1078-0432.CCR-08-1608>.
8. El-Khoueiry, A.B., Sangro, B., Yau, T., Crocenzi, T.S., Kudo, M., Hsu, C., Kim, T.Y., Choo, S.P., Trojan, J., Welling, T.H., et al. (2017). Nivolumab in patients with advanced hepatocellular carcinoma (CheckMate 040): an open-label, non-comparative, phase 1/2 dose escalation and expansion trial. *Lancet* 389, 2492–2502. [https://doi.org/10.1016/S0140-6736\(17\)31046-2](https://doi.org/10.1016/S0140-6736(17)31046-2).
9. Zhu, A.X., Finn, R.S., Edeline, J., Cattani, S., Ogasawara, S., Palmer, D., Verslype, C., Zagonel, V., Fartoux, L., Vogel, A., et al. (2018). Pembrolizumab in patients with advanced hepatocellular carcinoma previously treated with sorafenib (KEYNOTE-224): a non-randomised, open-label phase 2 trial. *Lancet Oncol.* 19, 940–952. [https://doi.org/10.1016/S1470-2045\(18\)30351-6](https://doi.org/10.1016/S1470-2045(18)30351-6).
10. Hagiwara, S., Nishida, N., and Kudo, M. (2023). Advances in Immunotherapy for Hepatocellular Carcinoma. *Cancers* 15, 2070. <https://doi.org/10.3390/cancers15072070>.
11. Fang, F., Xie, S., Chen, M., Li, Y., Yue, J., Ma, J., Shu, X., He, Y., Xiao, W., and Tian, Z. (2022). Advances in NK cell production. *Cell. Mol. Immunol.* 19, 460–481. <https://doi.org/10.1038/s41423-021-00808-3>.
12. Liu, E., Marin, D., Banerjee, P., Macapinlac, H.A., Thompson, P., Basar, R., Nassif Kerbauy, L., Overman, B., Thall, P., Kaplan, M., et al. (2020). Use of CAR-Transduced Natural Killer Cells in CD19-Positive Lymphoid Tumors. *N. Engl. J. Med.* 382, 545–553. <https://doi.org/10.1056/NEJMoa1910607>.
13. Myers, J.A., and Miller, J.S. (2021). Exploring the NK cell platform for cancer immunotherapy. *Nat. Rev. Clin. Oncol.* 18, 85–100. <https://doi.org/10.1038/s41571-020-0426-7>.
14. Arai, S., Meagher, R., Swearingen, M., Myint, H., Rich, E., Martinson, J., and Klingemann, H. (2008). Infusion of the allogeneic cell line NK-92 in patients with advanced renal cell cancer or melanoma: a phase I trial. *Cytotherapy* 10, 625–632. <https://doi.org/10.1080/14653240802301872>.
15. Maki, G., Klingemann, H.G., Martinson, J.A., and Tam, Y.K. (2001). Factors regulating the cytotoxic activity of the human natural killer cell line, NK-92. *J. Hematother. Stem Cell Res.* 10, 369–383. <https://doi.org/10.1089/152581601750288975>.
16. Mitra, B., Wang, J., Kim, E.S., Mao, R., Dong, M., Liu, Y., Zhang, J., and Guo, H. (2019). Hepatitis B Virus Precore Protein p22 Inhibits Alpha Interferon Signaling by Blocking STAT Nuclear Translocation. *J. Virol.* 93, e00196-19. <https://doi.org/10.1128/JVI.00196-19>.
17. Wang, L., Sun, Y., Song, X., Wang, Z., Zhang, Y., Zhao, Y., Peng, X., Zhang, X., Li, C., Gao, C., et al. (2021). Hepatitis B virus evades immune recognition via RNA adenosine deaminase ADAR1-mediated viral RNA editing in hepatocytes. *Cell. Mol. Immunol.* 18, 1871–1882. <https://doi.org/10.1038/s41423-021-00729-1>.
18. Wang, Y.X., Niklasch, M., Liu, T., Wang, Y., Shi, B., Yuan, W., Baumert, T.F., Yuan, Z., Tong, S., Nassal, M., and Wen, Y.M. (2020). Interferon-inducible MX2 is a host restriction factor of hepatitis B virus replication. *J. Hepatol.* 72, 865–876. <https://doi.org/10.1016/j.jhep.2019.12.009>.
19. Liu, N., Long, Y., Liu, B., Yang, D., Li, C., Chen, T., Wang, X., Liu, C., and Zhu, H. (2014). ISG12a mediates cell response to Newcastle disease viral infection. *Virology* 462–463, 283–294. <https://doi.org/10.1016/j.virol.2014.06.014>.
20. Xue, B., Yang, D., Wang, J., Xu, Y., Wang, X., Qin, Y., Tian, R., Chen, S., Xie, Q., Liu, N., and Zhu, H. (2016). ISG12a Restricts Hepatitis C Virus Infection through the Ubiquitination-Dependent Degradation Pathway. *J. Virol.* 90, 6832–6845. <https://doi.org/10.1128/JVI.00352-16>.
21. Deng, R., Zuo, C., Li, Y., Xue, B., Xun, Z., Guo, Y., Wang, X., Xu, Y., Tian, R., Chen, S., et al. (2020). The innate immune effector ISG12a promotes cancer immunity by suppressing the canonical Wnt/ $\beta$ -catenin signaling pathway. *Cell. Mol. Immunol.* 17, 1163–1179. <https://doi.org/10.1038/s41423-020-00549-9>.
22. Guo, M., Cao, W., Chen, S., Tian, R., Xue, B., Wang, L., Liu, Q., Deng, R., Wang, X., Wang, Z., et al. (2022). TRIM21 Regulates Virus-Induced Cell Pyroptosis through Polyubiquitination of ISG12a. *J. Immunol.* 209, 1987–1998. <https://doi.org/10.4049/jimmunol.2200163>.
23. Lee, S., Goyal, A., Perelson, A.S., Ishida, Y., Saito, T., and Gale, M., Jr. (2021). Suppression of hepatitis B virus through therapeutic activation of RIG-I and IRF3 signaling in hepatocytes. *iScience* 24, 101969. <https://doi.org/10.1016/j.isci.2020.101969>.
24. Yang, D., Zuo, C., Wang, X., Meng, X., Xue, B., Liu, N., Yu, R., Qin, Y., Gao, Y., Wang, Q., et al. (2014). Complete replication of hepatitis B virus and hepatitis C virus in a newly developed hepatoma cell line. *Proc. Natl. Acad. Sci. USA* 111, E1264–E1273. <https://doi.org/10.1073/pnas.1320071111>.
25. Datta, A., Deng, S., Gopal, V., Yap, K.C.H., Halim, C.E., Lye, M.L., Ong, M.S., Tan, T.Z., Sethi, G., Hooi, S.C., et al. (2021). Cytoskeletal Dynamics in Epithelial-Mesenchymal Transition: Insights into Therapeutic Targets for Cancer Metastasis. *Cancers* 13, 1882. <https://doi.org/10.3390/cancers13081882>.
26. Parker, N., and Porter, A.C.G. (2004). Identification of a novel gene family that includes the interferon-inducible human genes 6-16 and ISG12. *BMC Genom.* 5, 8. <https://doi.org/10.1186/1471-2164-5-8>.
27. Sarbassov, D.D., Guertin, D.A., Ali, S.M., and Sabatini, D.M. (2005). Phosphorylation and regulation of Akt/PKB by the rictor-mTOR complex. *Science* 307, 1098–1101. <https://doi.org/10.1126/science.1106148>.
28. Xue, B., Li, H., Guo, M., Wang, J., Xu, Y., Zou, X., Deng, R., Li, G., and Zhu, H. (2018). TRIM21 Promotes Innate Immune Response to RNA Viral Infection through Lys27-Linked Polyubiquitination of MAVS. *J. Virol.* 92, e00321-18. <https://doi.org/10.1128/JVI.00321-18>.
29. Taurin, S., Sandbo, N., Qin, Y., Browning, D., and Dulin, N.O. (2006). Phosphorylation of  $\beta$ -catenin by cyclic AMP-dependent protein kinase. *J. Biol. Chem.* 281, 9971–9976. <https://doi.org/10.1074/jbc.M508778200>.
30. He, X.C., Yin, T., Grindley, J.C., Tian, Q., Sato, T., Tao, W.A., Dirisina, R., Porter-Westpfahl, K.S., Hembree, M., Johnson, T., et al. (2007). PTEN-deficient intestinal stem cells initiate intestinal polyposis. *Nat. Genet.* 39, 189–198. <https://doi.org/10.1038/ng1928>.
31. Du, L., Lee, J.H., Jiang, H., Wang, C., Wang, S., Zheng, Z., Shao, F., Xu, D., Xia, Y., Li, J., et al. (2020).  $\beta$ -Catenin induces transcriptional expression of PD-L1 to promote glioblastoma immune evasion. *J. Exp. Med.* 217, e20191115. <https://doi.org/10.1084/jem.20191115>.
32. Allweiss, L., and Dandri, M. (2016). Experimental in vitro and in vivo models for the study of human hepatitis B virus infection. *J. Hepatol.* 64, S17–S31. <https://doi.org/10.1016/j.jhep.2016.02.012>.
33. Liu, Y.T., Tseng, T.C., Soong, R.S., Peng, C.Y., Cheng, Y.H., Huang, S.F., Chuang, T.H., Kao, J.H., and Huang, L.R. (2018). A novel spontaneous hepatocellular carcinoma mouse model for studying T-cell exhaustion in the tumor microenvironment. *J. Immunother. Cancer* 6, 144. <https://doi.org/10.1186/s40425-018-0462-3>.
34. Hu, J., Lin, Y.Y., Chen, P.J., Watashi, K., and Wakita, T. (2019). Cell and Animal Models for Studying Hepatitis B Virus Infection and Drug Development. *Gastroenterology* 156, 338–354. <https://doi.org/10.1053/j.gastro.2018.06.093>.
35. Yao, Z., Gao, G., Yang, J., Long, Y., Wang, Z., Hu, W., and Liu, Y. (2020). Prognostic Role of the Activated p-AKT Molecule in Various Hematologic Malignancies and Solid Tumors: A Meta-Analysis. *Front. Oncol.* 10, 588200. <https://doi.org/10.3389/fonc.2020.588200>.
36. Kong, X., Peng, H., Liu, P., Fu, X., Wang, N., and Zhang, D. (2023). Programmed death ligand 1 regulates epithelial-mesenchymal transition and cancer stem cell phenotypes in hepatocellular carcinoma through the serum and glucocorticoid kinase 2/ $\beta$ -catenin signaling pathway. *Cancer Sci.* 114, 2265–2276. <https://doi.org/10.1111/cas.15753>.

37. Sun, C., Sun, H.Y., Xiao, W.H., Zhang, C., and Tian, Z.G. (2015). Natural killer cell dysfunction in hepatocellular carcinoma and NK cell-based immunotherapy. *Acta Pharmacol. Sin.* 36, 1191–1199. <https://doi.org/10.1038/aps.2015.41>.
38. Sun, H., Huang, Q., Huang, M., Wen, H., Lin, R., Zheng, M., Qu, K., Li, K., Wei, H., Xiao, W., et al. (2019). Human CD96 Correlates to Natural Killer Cell Exhaustion and Predicts the Prognosis of Human Hepatocellular Carcinoma. *Hepatology* 70, 168–183. <https://doi.org/10.1002/hep.30347>.
39. Sun, C., Lan, P., Han, Q., Huang, M., Zhang, Z., Xu, G., Song, J., Wang, J., Wei, H., Zhang, J., et al. (2018). Oncofetal gene SALL4 reactivation by hepatitis B virus counteracts miR-200c in PD-L1-induced T cell exhaustion. *Nat. Commun.* 9, 1241. <https://doi.org/10.1038/s41467-018-03584-3>.
40. Gehring, A.J., Ho, Z.Z., Tan, A.T., Aung, M.O., Lee, K.H., Tan, K.C., Lim, S.G., and Bertoletti, A. (2009). Profile of tumor antigen-specific CD8 T cells in patients with hepatitis B virus-related hepatocellular carcinoma. *Gastroenterology* 137, 682–690. <https://doi.org/10.1053/j.gastro.2009.04.045>.
41. Fiscaro, P., Valdatta, C., Massari, M., Loggi, E., Biasini, E., Sacchelli, L., Cavallo, M.C., Silini, E.M., Andreone, P., Missale, G., and Ferrari, C. (2010). Antiviral intrahepatic T-cell responses can be restored by blocking programmed death-1 pathway in chronic hepatitis B. *Gastroenterology* 138, 682–693.e4. <https://doi.org/10.1053/j.gastro.2009.09.052>.
42. Lim, S.G., Baumert, T.F., Boni, C., Gane, E., Levrero, M., Lok, A.S., Maini, M.K., Terrault, N.A., and Zoulim, F. (2023). The scientific basis of combination therapy for chronic hepatitis B functional cure. *Nat. Rev. Gastroenterol. Hepatol.* 20, 238–253. <https://doi.org/10.1038/s41575-022-00724-5>.
43. Shimasaki, N., Jain, A., and Campana, D. (2020). NK cells for cancer immunotherapy. *Nat. Rev. Drug Discov.* 19, 200–218. <https://doi.org/10.1038/s41573-019-0052-1>.
44. Dogra, P., Rancan, C., Ma, W., Toth, M., Senda, T., Carpenter, D.J., Kubota, M., Matsumoto, R., Thapa, P., Szabo, P.A., et al. (2020). Tissue Determinants of Human NK Cell Development, Function, and Residence. *Cell* 180, 749–763.e13. <https://doi.org/10.1016/j.cell.2020.01.022>.
45. Freud, A.G., Mundy-Bosse, B.L., Yu, J., and Caligiuri, M.A. (2017). The Broad Spectrum of Human Natural Killer Cell Diversity. *Immunity* 47, 820–833. <https://doi.org/10.1016/j.immuni.2017.10.008>.
46. Jia, L., Gao, Y., He, Y., Hooper, J.D., and Yang, P. (2020). HBV induced hepatocellular carcinoma and related potential immunotherapy. *Pharmacol. Res.* 159, 104992. <https://doi.org/10.1016/j.phrs.2020.104992>.
47. Sun, Y., Yu, M., Qu, M., Ma, Y., Zheng, D., Yue, Y., Guo, S., Tang, L., Li, G., Zheng, W., et al. (2020). Hepatitis B virus-triggered PTEN/ $\beta$ -catenin/c-Myc signaling enhances PD-L1 expression to promote immune evasion. *Am. J. Physiol. Gastrointest. Liver Physiol.* 318, G162–G173. <https://doi.org/10.1152/ajpgi.00197.2019>.
48. Hsu, J., Hodgins, J.J., Marathe, M., Nicolai, C.J., Bourgeois-Daigneault, M.C., Trevino, T.N., Azimi, C.S., Scheer, A.K., Randolph, H.E., Thompson, T.W., et al. (2018). Contribution of NK cells to immunotherapy mediated by PD-1/PD-L1 blockade. *J. Clin. Invest.* 128, 4654–4668. <https://doi.org/10.1172/JCI99317>.
49. Böttcher, J.P., Bonavita, E., Chakravarty, P., Brees, H., Cabeza-Cabrero, M., Sammiceli, S., Rogers, N.C., Sahai, E., Zelenay, S., and Reis e Sousa, C. (2018). NK Cells Stimulate Recruitment of cDC1 into the Tumor Microenvironment Promoting Cancer Immune Control. *Cell* 172, 1022–1037.e14. <https://doi.org/10.1016/j.cell.2018.01.004>.
50. Barry, K.C., Hsu, J., Broz, M.L., Cueto, F.J., Binnewies, M., Combes, A.J., Nelson, A.E., Loo, K., Kumar, R., Rosenblum, M.D., et al. (2018). A natural killer-dendritic cell axis defines checkpoint therapy-responsive tumor microenvironments. *Nat. Med.* 24, 1178–1191. <https://doi.org/10.1038/s41591-018-0085-8>.
51. Wagner, A.K., Kadri, N., Tibbitt, C., van de Ven, K., Bagawath-Singh, S., Oliinyk, D., LeGresley, E., Campbell, N., Trittel, S., Riese, P., et al. (2022). PD-1 expression on mouse intratumoral NK cells and its effects on NK cell phenotype. *iScience* 25, 105137. <https://doi.org/10.1016/j.isci.2022.105137>.
52. Finn, R.S., Qin, S., Ikeda, M., Galle, P.R., Ducreux, M., Kim, T.Y., Kudo, M., Breder, V., Merle, P., Kaseb, A.O., et al. (2020). Atezolizumab plus Bevacizumab in Unresectable Hepatocellular Carcinoma. *N. Engl. J. Med.* 382, 1894–1905. <https://doi.org/10.1056/NEJMoa1915745>.
53. Terme, M., Ullrich, E., Aymeric, L., Meinhardt, K., Desbois, M., Delahaye, N., Viaud, S., Ryffel, B., Yagita, H., Kaplanski, G., et al. (2011). IL-18 induces PD-1-dependent immunosuppression in cancer. *Cancer Res.* 71, 5393–5399. <https://doi.org/10.1158/0008-5472.CAN-11-0993>.
54. Coënon, L., and Villalba, M. (2022). From CD16a Biology to Antibody-Dependent Cell-Mediated Cytotoxicity Improvement. *Front. Immunol.* 13, 913215. <https://doi.org/10.3389/fimmu.2022.913215>.
55. Park, J.E., Kim, S.E., Keam, B., Park, H.R., Kim, S., Kim, M., Kim, T.M., Doh, J., Kim, D.W., and Heo, D.S. (2020). Anti-tumor effects of NK cells and anti-PD-L1 antibody with antibody-dependent cellular cytotoxicity in PD-L1-positive cancer cell lines. *J. Immunother. Cancer* 8, e000873. <https://doi.org/10.1136/jitc-2020-000873>.
56. Qu, Y., Olsen, J.R., Yuan, X., Cheng, P.F., Levesque, M.P., Brokstad, K.A., Hoffman, P.S., Oyan, A.M., Zhang, W., Kalland, K.H., and Ke, X. (2018). Small molecule promotes  $\beta$ -catenin citrullination and inhibits Wnt signaling in cancer. *Nat. Chem. Biol.* 14, 94–101. <https://doi.org/10.1038/nchembio.2510>.

STAR★METHODS

KEY RESOURCES TABLE

REAGENT or RESOURCE	SOURCE	IDENTIFIER
<b>Antibodies</b>		
Rabbit anti-IGS12a	Sigma-Aldrich	Cat# SAB1408588; RRID: AB_10743854
Mouse anti-GAPDH	Merck Millipore	Cat# MAB374; RRID: AB_2107445
Mouse anti-Flag	Merck Millipore	Cat# F3165; RRID: AB_259529
Mouse anti-V5	Thermo Fisher Scientific	Cat# R960-25; RRID: AB_2556564
Mouse anti-HA	Cell Signaling Technology	Cat# 3724S; RRID: AB_1549585
Rabbit anti-β-Catenin	Cell Signaling Technology	Cat# 8480S; RRID: AB_11127855
Rabbit anti-p-β-Catenin (Ser552)	Cell Signaling Technology	Cat# 5651S; RRID: AB_10831053
Rabbit anti-PD-L1	Proteintech	Cat#17952-1-AP; RRID: AB_10597552
Rabbit anti-AKT	Cell Signaling Technology	Cat# 4691S; RRID: AB_915783
Rabbit anti-p-AKT (Ser473)	Cell Signaling Technology	Cat# 4060S; RRID: AB_2315049
Mouse anti-mTOR	Santa Cruz Biotechnology	Cat# sc-517464
Mouse anti-p-mTOR (Ser2448)	Santa Cruz Biotechnology	Cat# sc-293133; RRID: AB_2861149
Mouse anti-HBsAg	Santa Cruz Biotechnology	Cat# sc-53300; RRID: AB_629596
Mouse anti-HBcAg	Santa Cruz Biotechnology	Cat# sc-23945; RRID: AB_627701
Mouse anti-β-actin	Sigma-Aldrich	Cat# A5316; RRID: AB_476743
Rabbit anti-STAT1	Cell Signaling Technology	Cat# 14994; RRID: AB_2737027
Rabbit anti-p-STAT1 (Tyr701)	Cell Signaling Technology	Cat# 9167; RRID: AB_561284
Rabbit anti-STAT2	Cell Signaling Technology	Cat# 72604; RRID: AB_2799824
Rabbit anti-p-STAT2 (Tyr690)	Cell Signaling Technology	Cat# 88410; RRID: AB_2800123
Rabbit anti-Lamin B1	Cell Signaling Technology	Cat# 12586; RRID: AB_2650517
InVivoSIM anti-human PD-1	Bio X Cell	Cat# SIM0003; RRID: AB_2894724
InVivoSIM anti-human PD-L1	Bio X Cell	Cat# SIM0009; RRID: AB_2894730
InVivoPlus human IgG1 isotype control	Bio X Cell	Cat# BP0297
RecombiMAb human IgG4 (S228P) isotype control	Bio X Cell	Cat# CP147
Goat anti-mouse IgG (HRP-linked)	Merck Millipore	Cat# AP124P; RRID: AB_90456
Goat anti-rabbit IgG (HRP-linked)	Merck Millipore	Cat# AP132P; RRID: AB_90264
HRP-conjugated goat anti-human IgG	Sangon Biotech	Cat# D110150; RRID: AB_2876788
Alexa Fluor <sup>®</sup> 555 Phalloidin	Cell Signaling Technology	Cat# 8953S
Mouse anti-CD56	Proteintech	Cat# 60238-1-Ig; RRID: AB_2881361
Brilliant Violet 421 <sup>™</sup> anti-human CD274 (B7-H1, PD-L1) Antibody	BioLegend	Cat# 329714; RRID: AB_2563852
PE anti-human CD279 (PD-1) Antibody	BioLegend	Cat# 329906; RRID: AB_940481
Rabbit anti-Histone H3	Cell Signaling Technology	Cat# 4620S; RRID: AB_1904005
Normal rabbit IgG	Cell Signaling Technology	Cat# 2729S; RRID: AB_1031062
<b>Bacterial and virus strains</b>		
<i>Escherichia coli</i> DH5α competent cells	Lab stock	N/A
NDV D817	Dr. Joseph Peiris (University of Hongkong)	N/A
Lentivirus-expressing LT-shCtrl	This paper	N/A

(Continued on next page)

**Continued**

REAGENT or RESOURCE	SOURCE	IDENTIFIER
Lentivirus-expressing LT-shISG12a	This paper	N/A
Lentivirus-expressing Flag vector	This paper	N/A
Lentivirus-expressing Flag-PD1	This paper	N/A
<b>Biological samples</b>		
Formed tumors in NCG mice	This paper	N/A
<b>Chemicals, peptides, and recombinant proteins</b>		
Puromycin	Thermo Fisher Scientific	Cat# A1113803
Nitazoxanide	MedChemExpress	Cat# HY-B0217
TRlzol reagent	Thermo Fisher Scientific	Cat# 15596018
Proteinase inhibitor cocktail	Thermo Fisher Scientific	Cat# 7843
RIPA buffer	Thermo Fisher Scientific	Cat# 89900
IP lysis buffer	Thermo Fisher Scientific	Cat# 87787
Insulin-transferrin-selenium	Thermo Fisher Scientific	Cat# 41400-045
MEM non-essential amino acids solution	Thermo Fisher Scientific	Cat# 11140-050
Inositol	Sigma-Aldrich	Cat# I7508
Folic acid	Sigma-Aldrich	Cat# F8758
$\beta$ -Mercaptoethanol	Sigma-Aldrich	Cat# M3148
rhIL-2	Sigma-Aldrich	Cat# SRP3085
4% paraformaldehyde	DINGGUO CHANGSHENG BIOTECHNOLOGY C.LTD.	Cat# AR-0211
0.2% Triton X-100	DINGGUO CHANGSHENG BIOTECHNOLOGY C.LTD.	Cat# AR-0341
DAPI	Vector Laboratories	Cat# H-1200-10
Blue Plus <sup>®</sup> II Western Marker	Transgen Biotech	Cat# DM111-02
DAB	BOSTER	Cat# AR1022
Hematoxylin	BOSTER	Cat# AR0005
<b>Critical commercial assays</b>		
KOD-Plus-Neo	TOYOBO	Cat# KOD-401
PrimeScript <sup>™</sup> RT reagent Kit with gDNA Eraser kit	Takara	Cat# RR047A
Nuclear and Cytoplasmic Protein Extraction Kit	Sangon Biotech	Cat# C510001
SuperSignal <sup>®</sup> West Pico Chemiluminescent Substrate	Thermo Fisher Scientific	Cat# 34578
SYBR <sup>®</sup> Premix Ex Taq <sup>™</sup> II (Tli RNaseH Plus)	Takara	Cat# RR820A
Diagnostic Kit for HBsAg (ELISA)	SHANGHAI KEHUA BIO-ENGINEERING CO., LTD.	N/A
Diagnostic Kit for HBeAg (ELISA)	SHANGHAI KEHUA BIO-ENGINEERING CO., LTD.	N/A
Dual-Luciferase <sup>®</sup> Reporter 1000 Assay System	Promega	Cat# E1980
SimpleChIP <sup>®</sup> Enzymatic Chromatin IP Kit (Agarose Beads)	Cell Signaling Technology	Cat# 9002

(Continued on next page)

**Continued**

REAGENT or RESOURCE	SOURCE	IDENTIFIER
<i>Experimental models: Cell lines</i>		
HLCZ01	Lab stock (Yang et al. Proc Natl Acad Sci U S A 111, E1264-1273)	RRID: CVCL_1J92
Huh7	Chen Liu (Yale School of Medicine)	RRID: CVCL_0336
HepG2.2.15	Chen Liu (Yale School of Medicine)	RRID: CVCL_L855
NK-92	ATCC	RRID: CVCL_2142
HEK293T	ATCC	RRID: CVCL_0063
<i>Experimental models: Organisms/strains</i>		
NCG mouse	GemPharmatech	RRID: IMSR_GPT:T001475
<i>Oligonucleotides</i>		
shRNA targeting sequence: LT-shCtrl: TAAGGTAAAGTCGCCCTCG	This paper	N/A
shRNA targeting sequence: LT-sh/SG12a: CTGGACTCTCCGGATTGAC	This paper	N/A
Primers used for plasmid construction, see <a href="#">Table S3</a>	This paper	N/A
Primers used for qRT-PCR, see <a href="#">Table S4</a>	This paper	N/A
<i>Recombinant DNA</i>		
p3×Flag vector	Sigma-Aldrich	Cat# E7908; RRID: Addgene_73391
p3×Flag-AKT	This paper	N/A
p3×Flag-CTNNB1	This paper	N/A
p3×Flag-S552A	This paper	N/A
p3×Flag-S552D	This paper	N/A
pGreenPuro™ shRNA cloning and expression lentivector	System Biosciences	Cat# SI505A-1
LT-shCtrl	This paper	N/A
LT-sh/SG12a	This paper	N/A
pCDH-CMV-MCS-EF1 lentivector	System Biosciences	Cat# CD513B-1
LT-Flag vector	This paper	N/A
LT-Flag-PD1	This paper	N/A
psPAX2	Addgene	Cat# 12260; RRID: Addgene_12260
pMD2.G	Addgene	Cat# 12259; RRID: Addgene_12259
pRL-CMV	Addgene	Cat# 41729; RRID: Addgene_41729
<i>Software and algorithms</i>		
GraphPad Prism 8.0	GraphPad	<a href="https://www.graphpad.com/">https://www.graphpad.com/</a>
FlowJo V10.0.7 software	Becton, Dickinson & Company	<a href="https://www.flowjo.com/">https://www.flowjo.com/</a>
Image Lab 5.2	BIO-RAD	<a href="https://www.bio-rad.com/zh-cn/product/image-lab-software?ID=KRE6P5E8Z">https://www.bio-rad.com/zh-cn/product/image-lab-software?ID=KRE6P5E8Z</a>
ImageJ software	National Institutes of Health	<a href="https://ImageJ.en.softonic.com/mac">https://ImageJ.en.softonic.com/mac</a>
<i>Other</i>		
DMEM	Thermo Fisher Scientific	Cat# C11965500BT
MEM $\alpha$ medium	Thermo Fisher Scientific	Cat# 12000063
DMEM/F12 medium	Thermo Fisher Scientific	Cat# C11330500BT
FBS	Thermo Fisher Scientific	Cat# 10270-106
Horse serum	Thermo Fisher Scientific	Cat# 26050088
Normal goat serum	Thermo Fisher Scientific	Cat# 16210064

(Continued on next page)

**Continued**

REAGENT or RESOURCE	SOURCE	IDENTIFIER
Penicillin-streptomycin	Thermo Fisher Scientific	Cat# 15140122
Opti-MEM™ I medium	Thermo Fisher Scientific	Cat# 31985088
Lipofectamine™ 2000	Thermo Fisher Scientific	Cat# 11668019

**RESOURCE AVAILABILITY****Lead contact**

Further information and requests for resources and reagents should be directed to and will be fulfilled by the lead contact, Haizhen Zhu ([hy0206218@hainmc.edu.cn](mailto:hy0206218@hainmc.edu.cn)).

**Materials availability**

This study did not generate new unique reagents. All the cell lines used in this manuscript will be made available upon request. A material transfer agreement will be required prior to sharing of materials.

**Data and code availability**

- Date: Data reported in this paper will be shared by the [lead contact](#) upon request.
- Code: This paper does not report original code.
- All other requests: Any additional information required to reanalyze the data reported will be shared by the [lead contact](#) upon request.

**EXPERIMENTAL MODEL AND STUDY PARTICIPANT DETAILS****Ethics approval and consent to participate**

Animal experiments were in accordance with protocols approved by the Animal Care and Experiment Committee of Hunan University. All applicable international, national, and/or institutional guidelines for the care and use of animals were followed. TCGA database belongs to public databases, and the patients involved in this database have obtained ethical approval. Our study is based on open source in TCGA database, so there are no ethical issues and other conflicts of interest.

**Cell lines**

The human hepatic cell line HLCZ01 (RRID: CVCL\_1J92) was isolated and stored in our laboratory,<sup>24</sup> the human hepatic cell line Huh7 (RRID: CVCL\_0336) and HepG2.2.15 (RRID: CVCL\_L855) were kindly provided by Chen Liu (Yale School of Medicine), and the human embryonic kidney fibroblasts HEK293T (RRID: CVCL\_0063) and the natural killer cell line NK-92 (RRID: CVCL\_2142) were purchased from American Type Culture Collection (Manassas, VA, USA).

**Mice**

A total of 63 six-week-old male NCG mice (Strain NO. T001475) that purchased from GemPharmatech (Nanjing, China). Mice were housed in a pathogen-free environment at animal care facility of Hunan University at 25°C and 40–60% humidity with a 12-h light/dark cycle and free access to standard sterile food and water. Protocol used for animal experiments was approved by the Animal Care and Experiment Committee of Hunan University.

**METHOD DETAILS****Cell culture**

HLCZ01 cells were cultivated in DMEM/F12 medium (Cat# C11330500BT, Thermo Fisher Scientific, Waltham, MA, USA) supplemented with 10% (v/v) fetal bovine serum (FBS) (Cat# 10270-106, Thermo Fisher Scientific), penicillin-streptomycin (Cat# 15140122, Thermo Fisher Scientific), and insulin-transferrin-selenium (Cat# 41400-045, Thermo Fisher Scientific). Huh7, HepG2.2.15, and HEK293T cells were cultivated in DMEM medium (Cat# C11965500BT, Thermo Fisher Scientific) supplemented with 10% (v/v) FBS, MEM non-essential amino acids solution (Cat# 11140-050, Thermo Fisher Scientific), and penicillin-streptomycin. NK-92 cells were cultivated in MEM $\alpha$  medium (Cat# 12000063, Thermo Fisher Scientific) supplemented with 7.5% (v/v) heat-inactivated FBS (Cat# 10270-106, Thermo Fisher Scientific), 7.5% (v/v) heat-inactivated horse serum (Cat# 26050088, Thermo Fisher Scientific), 0.2 mM inositol (Cat# I7508, Sigma-Aldrich, St. Louis, MO, USA), 0.02 mM folic acid (Cat# F8758, Sigma-Aldrich), 0.1 mM  $\beta$ -mercaptoethanol (Cat# M3148, Sigma-Aldrich), 100 U/ml rhIL-2 (Cat# SRP3085, Sigma-Aldrich), and penicillin-streptomycin. Cells were used within ten passages, authenticated by STR profiling, passaged for an average of three days, and tested routinely before use to avoid mycoplasma contamination. Cell transfection with plasmids was conducted using Lipofectamine 2000 (Cat# 11668019, Thermo Fisher Scientific) in Opti-MEM I medium (Cat# 31985088, Thermo Fisher Scientific). Cell proliferation was determined

by counting using a blood counting chamber. Nitazoxanide (NTZ) (Cat# HY-B0217, MedChemExpress) was used to block the expression of  $\beta$ -Catenin in cancer cells.<sup>56</sup>

### Plasmids construction

Gene expression plasmids of *ISG12a* and *TRIM21* were constructed in our previous study,<sup>20,28</sup> and protocols used for plasmid construction were detailed in our previous research.<sup>21</sup> Reverse transcription PCR of total RNA was performed using PrimeScript RT reagent Kit with gDNA Eraser kit (Cat# RR047A, Takara, Kusatsu, Japan), and DNA sequences of open reading frames (ORFs) were obtained using high-fidelity PCR kit KOD-Plus-Neo kit (Cat# KOD-401, TOYOBO, Tokyo, Japan). Primers used for plasmid construction of *AKT* and *CTNNB1* based on p3 $\times$  Flag-CMV-14 vector (Sigma-Aldrich) are listed in [Table S3](#) cDNA used for constructing *PD-1* plasmid (LT-Flag-*PD1*) was obtained from K562 cells and inserted pCDH-CMV-MCS-EF1 lentivector (Cat# CD513B-1, SBI, Palo Alto, CA, USA) modified with FLAG tag, and primers are listed in [Table S3](#). Promoter plasmid pGL3-*CD274* was constructed in our previous study.<sup>21</sup> Gene silencing plasmids were constructed using pGreenPuro shRNA cloning and expression lentivector (Cat# SI505A-1, SBI). Targets used for silencing gene expression are listed in [key resources table](#). Plasmids were amplified in *Escherichia coli* DH5 $\alpha$  competent cells.

### Lentiviral package and infection

A certain number of HEK293T cells were seeded into 100 mm dishes to ensure that the cell coverage reaches 60–70% after cultivation for 24 h. 8.0  $\mu$ g of gene silencing or expression plasmids, 8.0  $\mu$ g of lentiviral packaging plasmid psPAX2 (Cat# 12260, Addgene, Watertown, MA, USA), and 2.7  $\mu$ g of envelope plasmid pMD2.G (Cat# 12259, Addgene) into 300  $\mu$ L of Opti-MEM I medium. 18  $\mu$ L of Lipofectamine 2000 was mixed into 300  $\mu$ L of Opti-MEM I medium and incubated at room temperature for 5 min. Then plasmids and Lipofectamine 2000 were mixed together and incubated at room temperature for 20 min. The mixture was added into the medium of HEK293T cells for transfection. 48 h later, cell supernatants containing viral particles were collected, filtered with 0.45  $\mu$ m filters. Lentivirus was added into culture medium of cells at approximately 30–40% coverage. 72 h post viral infection, puromycin (Cat# A1113803, Thermo Fisher Scientific) was added to screen the stably infected cells.

### NDV production

NDV was kindly provided by Dr. Joseph Peiris (University of Hongkong). NDV was amplified in Huh7 cells at MOI of 0.01. Supernatants containing virus of Huh7 cells were harvested and purified by centrifugation, and the viral titers were determined by TICD50.

### Qualitative real-time PCR (qRT-PCR)

Total RNA was extracted from cells using TRIzol reagent (Cat# 15596018, Thermo Fisher Scientific). To avoid genomic DNA contamination, reverse transcription PCR was performed using PrimeScript RT reagent Kit with gDNA Eraser. qRT-PCR was conducted using SYBR Premix Ex Taq II (Tli RNaseH Plus) (Cat# RR820A, Takara) with an ABI7500 thermocycler (Thermo Fisher Scientific). Primers used for qRT-PCR are listed in [Table S4](#) and synthesized at Sangon Biotech, and *GAPDH* was the internal control.

### HBV infection of cell culture

Protocol for constructing HBV-infected HLCZ01 cells was reported in our previous research.<sup>24</sup> In brief, the supernatants of cultured HepG2.2.15 cells were collected and filtered using 0.22  $\mu$ m filter membranes, which were further purified and concentrated by conducting sucrose gradient centrifugation. HLCZ01 cells were inoculated overnight with the filtered supernatants at a multiplicity of infection of 20 genome equivalents per cell. HBV-infected HLCZ01 cells were maintained in DMEM/F12 medium supplemented with 10% (v/v) FBS, penicillin-streptomycin, and insulin-transferrin-selenium.

### Immunoblots and co-immunoprecipitation (co-IP)

Whole cell lysates for immunoblots were extracted using RIPA buffer (Cat# 89900, Thermo Fisher Scientific), whole cell lysates for co-IP were extracted using IP lysis buffer (Cat# 7843, Thermo Fisher Scientific), and protein in cell cytoplasm and cell nuclei were extracted using the Nuclear and Cytoplasmic Protein Extraction Kit (Cat# C510001, Sangon Biotech, Shanghai, China). Protocols used for immunoblots and co-IP were detailed in our previous research.<sup>21</sup> Images of protein bands were detected using SuperSignal West Pico Chemiluminescent Substrate (Cat# 34578, Thermo Fisher Scientific) and analyzed using software Image Lab 5.2 (BIO-RAD, CA, USA). Following antibodies were used for immunoblots and co-IP: *ISG12a* (1:1000, Cat# SAB1408588, Sigma-Aldrich), *GAPDH* (1:2000, clone 6C5, Cat# MAB374, Merck Millipore, Darmstadt, Germany), Flag (1:5000, clone M2, Cat# F3165, Sigma-Aldrich), V5 (1:2000, Cat# R960-25, Thermo Fisher Scientific), HA (1:1000, clone C29F4, Cat# 3724S, Cell Signaling Technology, Danvers, MA, USA),  $\beta$ -Catenin (1:1000, clone D10A8, Cat# 8480S, Cell Signaling Technology), p- $\beta$ -Catenin (1:1000, clone D8E11, Cat# 5651S, Cell Signaling Technology), PD-L1 (1:250, Cat# 17952-1-AP, Proteintech, Rosemont, IL, USA), AKT (1:1000, clone C67E7, Cat# 4691S, Cell Signaling Technology), p-AKT (1:1000, clone D9E, Cat# 4060S, Cell Signaling Technology), mTOR (1:500, clone 30, Cat# sc-517464, Santa Cruz Technology, Dallas, TX, USA), p-mTOR (1:500, clone 59, Cat# sc-293133, Santa Cruz Technology), HBsAg (1:250, clone 1025, Cat# sc-53300, Santa Cruz Technology), HbcAg (1:250, clone C1-5, Cat# sc-23945, Santa Cruz Technology),  $\beta$ -actin (1:5000, clone AC-74, Cat# A5316, Sigma-Aldrich), InVivoSIM anti-human PD-1 (Nivolumab Biosimilar) (1:500, clone Nivolumab, Cat# SIM0003, Bio X Cell, NH, USA), goat anti-mouse IgG (HRP-linked) (1:5000, Cat# AP124P, Merck Millipore), goat anti-rabbit IgG (HRP-linked) (1:5000,

Cat# AP132P, Merck Millipore), and HRP-conjugated goat anti-human IgG (1:500, Cat# D110150, Sangon Biotech). The potential interacting proteins were determined by mass spectrometry. Density of proteins was determined using ImageJ software (National Institutes of Health, USA).

### Immunofluorescence staining

Alexa Fluor 555 Phalloidin (Cat# 8953S, Cell Signaling Technology) was commercially obtained and used to stain F-actin in cells. In brief, an average of  $1.5 \times 10^5$  cells were seeded into a 35-mm confocal dish. After cultivation for 48 h, cells were rinsed with ice-cold PBS, fixed with 4% paraformaldehyde (Cat# AR-0211, DINGGUO CHANGSHENG BIOTECHNOLOGY C.LTD., Beijing, China) at 4°C for 30 min, permeabilized with 0.2% Triton X-100 (Cat# AR-0341, DINGGUO CHANGSHENG BIOTECHNOLOGY C.LTD.) for 10 min, and blocked with normal goat serum (Cat# 16210064, Thermo Fisher Scientific) for 1 h. Then, cells were incubated with 0.33  $\mu$ M phalloidin at room temperature for 15 min, and cell nucleus were stained with DAPI (Cat# H-1200-10, Vector Laboratories, CA, USA) for 5 min. Images of stained cells were captured using a TI-E + A1 SI confocal microscope (Nikon, Tokyo, Japan).

### Immunohistochemistry (IHC) staining

Protocol used for IHC staining was described in our previous research.<sup>21</sup> Following antibodies were used to examine NK cell infiltration in mice tumors: CD56 (1:1000, clone 1E8C9, Cat# 60238-1-Ig, Proteintech) and goat anti-mouse IgG (HRP-linked) (1:2000, Cat# AP124P, Merck Millipore). After antibody incubation, slices were stained with DAB (Cat# AR1022, BOSTER, Wuhan, China), and hematoxylin (Cat# AR0005, BOSTER) was used to counterstain the nucleus. Images of IHC staining of tissue slices were captured using an IX71 inverted light microscope (Olympus, Tokyo, Japan).

### Wound-healing assay

Cells in the logarithmic phase were seeded in a six-well plate at 50–60% confluence. After cultivation using medium containing 10% (v/v) FBS in an incubator with 5% CO<sub>2</sub> at 37°C for 24 h, cells were cultivated using serum-free medium for another 24 h. Then, a wound was generated in the adherent cell monolayer using a standard 10- $\mu$ L pipette tip and a ruler, and cells were continually cultivated in serum-free medium for 48 h. The wound-healing process of cells at different timepoints were recorded using an inverted light microscope IX71.

### Flow cytometry

Expression levels of surface PD-1 on NK-92 cells and PD-L1 on hepatic cancer cells were examined by flow cytometry, and detailed protocol was described in our previous research.<sup>21</sup> Following antibodies were used for flow cytometry analysis: PE anti-human CD279 (PD-1) Antibody (1:200, clone EH12.2H7, Cat# 329906, BioLegend, San Diego, CA, USA) and Brilliant Violet 421 anti-human CD274 (B7-H1, PD-L1) Antibody (1:100, clone 29E.2A3, Cat# 329714, BioLegend). Flow cytometry for surface PD-1 was conducted using BD FACSAria II flow cytometer (BD Bioscience, San Jose, CA, USA), and the data were analyzed using FlowJo V10.0.7 software (FlowJo, LLC, San Jose, CA, USA).

### ELISA

HBsAg and HBeAg level were determined by ELISA using Diagnostic Kit for HBsAg (ELISA) and Diagnostic Kit for HBeAg (ELISA) (SHANGHAI KEHUA BIO-ENGINEERING CO., LTD., Shanghai, China), respectively. Positive and negative controls were involved in assays. The simplified protocol is listed below: Samples and controls were incubated with anti-HBsAg and HBeAg pre-treated microplates, respectively; Enzyme-binding substrates were mixed and incubated for different times; Chromogenic solution and stop solution were sequentially added for following measurement at 450 nm wavelength on a microplate reader SENERGY HTX (BIOTEK, Palo Alto, CA, USA).

### Dual luciferase reporter assay

Dual luciferase reporter assays were applied to analyze the activity of PD-L1 promoter. In brief, 750 ng of gene expression plasmids or vector control along with 250 ng of promoter plasmid pGL3-CD274 (Firefly luciferase), 10 ng of pRL-MCV plasmid (Renilla luciferase) (Promega) accompanying with 3  $\mu$ L of Lipofectamine 2000 were co-transfected into cells in each well of a 12-well cell culture plate for 36 h. pRL-CMV was used as an internal control plasmid. Dual-Luciferase Reporter 1000 Assay System (Promega) was used to determine the transcriptional activity of the promoter. Fold change of luciferase expression was calculated based on the ratio of the Firefly and Renilla luciferase activities.

### Chromatin immunoprecipitation (ChIP)

Protocol used for ChIP staining was described in our previous research.<sup>21</sup> SimpleChIP Enzymatic Chromatin IP Kit (Agarose Beads) (Cat# 9002, Cell Signaling Technology, Danvers, MA, USA) based on enzymatic digestion of genomic DNA was used in experiments. Relative level of binding DNA sequences to transcription factors was determined by RT-PCR, and primers are listed below: AGAAGTTCAG CGCGGGATAA (forward) and GCCCTTTTGAAGCTTTGGGT (reverse). Following antibodies were used to conduct ChIP assays: Histone H3 (1:50, clone D2B12, Cat# 4620S, Cell Signaling Technology), rabbit anti- $\beta$ -Catenin (1:25, clone D10A8, Cat# 8480S, Cell Signaling Technology), and normal rabbit IgG (Cat# 2729S, Cell Signaling Technology).

### HCC in The Cancer Genome Atlas (TCGA) database

FPKM-UQ data of HCC in TCGA database were used for analysis. Sample inclusion criteria are as follows: (1) HBV-infected and non-HBV/non-HCV-infected HCC; (2) No anticancer therapy (surgery, immunotherapy, radiotherapy, and chemotherapy) prior to liver cancer surgery for which specimens were obtained; (3) Complete clinicopathological data. FPKM-UQ data were converted as  $\log_2$  values, and the detailed information of samples used in this study are listed in [Table S1](#).

### Xenograft experiment

Cells in 150  $\mu\text{L}$  of sterile PBS were subcutaneously injected into the back of the right hind legs of an NCG mouse. Tumors grew for at least 10 days before randomizing into untreated control PBS or NK-92 group as well as ICB or IgG group with 5–6 mice per group. Then,  $5 \times 10^6$  NK cells were administrated into each mouse by intraperitoneal injection at the indicated timepoints presented in images, and 200  $\mu\text{g}$  of antibodies or IgGs in 400  $\mu\text{L}$  of sterile PBS by intraperitoneal injection at indicated timepoints. Mice in this study were sacrificed when they experienced a sharp decrease in activity, water and diet intake, and tumors were harvested for the follow-up analyses. Investigators were blinded during experiments. Following antibodies were used in animal experiments: InVivoSIM anti-human PD-L1 (Atezolizumab Biosimilar) (clone Atezolizumab, Cat# SIM0009, Bio X Cell), InVivoPlus human IgG1 isotype control (Cat# BP0297, Bio X Cell), InVivoSIM anti-human PD-1 (Nivolumab Biosimilar) (clone Nivolumab, Cat# Cat# SIM0003, Bio X Cell), and RecombiMAb human IgG4 (S228P) isotype control (Cat# CP147, Bio X Cell).

### QUANTIFICATION AND STATISTICAL ANALYSIS

GraphPad Prism 8.0 (GraphPad, San Diego, CA, USA) was used to conduct statistical analyses and draw statistical graphs. Experiments were independently repeated two or three times with similar results, and representative images are shown in figures. Pearson correlation ( $r$ ) analysis (two-tailed) was using to analyze correlation between the levels of ISG12a and NK cell signatures or TRIM21. Kaplan-Meier analysis (log rank test) was performed to determine the correlation between ISG12a level and 5-year overall survival rate, and the high and low levels of ISG12a transcript were determined according to the median value. Data were analyzed by unpaired two-sided Student's  $t$  tests or one-way ANOVA, and are presented as mean  $\pm$  SD or mean  $\pm$  SEM with at least three biological replicates or three replicate experiments. Significance levels: \*, #  $p < 0.05$ , \*\*, ##  $p < 0.01$ , \*\*\*, ###  $p < 0.001$ , and not significant (ns).